REPORT DOCUMENTATION PAGE

Form Approved
OMB No. 0704-0188

PLEASE DO NOT RETURN YOUR FORM TO THE ABOVE ORGANIZATION.

1. REPORT DATE *(DD-MM-YYYY)*	2. REPORT TYPE	3. DATES COVERED *(From - To)*
6-06-2006	Journal Article (refereed)	

4. TITLE AND SUBTITLE
Interannual Variability of Tehuantepec Eddies

5a. CONTRACT NUMBER

5b. GRANT NUMBER

5c. PROGRAM ELEMENT NUMBER
PE0601153N

6. AUTHOR(S)
Luis Zamudio, Harley E. Hurlburt, E. Joseph Metzger, Steven L. Morey, James J. O'Brien, Charles Tilburg, and Jorge Zavala-Hidalgo

5d. PROJECT NUMBER

5e. TASK NUMBER

5f. WORK UNIT NUMBER
73-5732-04

7. PERFORMING ORGANIZATION NAME(S) AND ADDRESS(ES)
Naval Research Laboratory
Oceanography Division
Stennis Space Center, MS 39529-5004

8. PERFORMING ORGANIZATION REPORT NUMBER
NRL/JA/7304-03-52

9. SPONSORING/MONITORING AGENCY NAME(S) AND ADDRESS(ES)
Office of Naval Research
800 N. Quincy St.
Arlington, VA 22217-5660

10. SPONSOR/MONITOR'S ACRONYM(S)
ONR

11. SPONSOR/MONITOR'S REPORT NUMBER(S)

12. DISTRIBUTION/AVAILABILITY STATEMENT
Approved for public release, distribution is unlimited.

13. SUPPLEMENTARY NOTES

14. ABSTRACT

TOPEX/Poseidon satellite altimeter observations and the Naval Research Laboratory Layered Ocean Model simulations show interannual variability in the number and intensity of Tehuantepec eddies off the Mexican southwest coast. Analysis of the results illustrates that downwelling coastally trapped waves, which are generated in the equatorial Pacific, play a crucial role in the modulation and generation of Tehuantepec eddies and a paradigm in which the generation and modulation of Tehuantepec eddies is not exclusively explained in terms of the strong and intermittent Tehuan tepec wind events. In fact, the results show anticyclonic eddy formation during periods of calm Tehuantepec winds. That is specifically exemplified by the formation of two anticyclonic Tehuantepec eddies during a five-month period of weak Gulf of Tehuantepec winds during summer of 1997. Furthermore, the satellite-observed and NLOM-simulated proliferation of Tehuantepec eddies during El Niño years is explained by the corresponding increase in downwelling coastally trapped waves and a lack of increases in the number and streugth of Tehuantepec wind events during El Niño years.

15. SUBJECT TERMS
Tehuantepec eddies; downwelling; coastally trapped waves

16. SECURITY CLASSIFICATION OF:			17. LIMITATION OF ABSTRACT	18. NUMBER OF PAGES	19a. NAME OF RESPONSIBLE PERSON
a. REPORT	b. ABSTRACT	c. THIS PAGE			Harley Hurlburt
Unclassified	Unclassified	Unclassified	UL	21	19b. TELEPHONE NUMBER *(Include area code)* (228) 688-4626

Interannual variability of Tehuantepec eddies

Luis Zamudio, Harley E. Hurlburt, E. Joseph Metzger, Steven L. Morey,
James J. O'Brien, Charles Tilburg, and Jorge Zavala-Hidalgo

Interannual variability of Tehuantepec eddies

Luis Zamudio,[1] Harley E. Hurlburt,[2] E. Joseph Metzger,[2] Steven L. Morey,[1] James J. O'Brien,[1] Charles Tilburg,[3] and Jorge Zavala-Hidalgo[4]

Received 21 July 2005; revised 22 December 2005; accepted 26 January 2006; published 2 May 2006.

[1] TOPEX/Poseidon satellite altimeter observations and the Naval Research Laboratory Layered Ocean Model simulations show interannual variability in the number and intensity of Tehuantepec eddies off the Mexican southwest coast. Analysis of the results illustrates that downwelling coastally trapped waves, which are generated in the equatorial Pacific, play a crucial role in the modulation and generation of Tehuantepec eddies and a dominant role in Tehuantepec eddy interannual variability. This introduces a new paradigm in which the generation and modulation of Tehuantepec eddies is not exclusively explained in terms of the strong and intermittent Tehuantepec wind events. In fact, the results show anticyclonic eddy formation during periods of calm Tehuantepec winds. That is specifically exemplified by the formation of two anticyclonic Tehuantepec eddies during a 5-month period of weak Gulf of Tehuantepec winds during summer of 1997. Furthermore, the satellite-observed and NLOM-simulated proliferation of Tehuantepec eddies during El Niño years is explained by the corresponding increase in downwelling coastally trapped waves and a lack of increase in the number and strength of Tehuantepec wind events during El Niño years.

Citation: Zamudio, L., H. E. Hurlburt, E. J. Metzger, S. L. Morey, J. J. O'Brien, C. E. Tilburg, and J. Zavala-Hidalgo (2006), Interannual variability of Tehuantepec eddies, *J. Geophys. Res.*, *111*, C05001, doi:10.1029/2005JC003182.

1. Introduction

[2] Previous studies have shown that the generation of oceanic Tehuantepec eddies off the Mexican southwest coast is due to intermittent strong offshore winds that can exist in the Gulf of Tehauntepec (GT) mainly during the boreal cold season (fall–winter) [*Clarke*, 1998; *McCreary et al.*, 1989; *Lavín et al.*, 1992; *Giese et al.*, 1994; *Müller-Karger and Fuentes-Yaco*, 2000]. The GT high wind events are associated with the arrival of high pressure following the passage of atmospheric cold fronts into the Gulf of Mexico [*Barton et al.*, 1993; *Trasviña et al.*, 1995; *Bourassa et al.*, 1999; *Chelton et al.*, 2000a]. This high atmospheric pressure, combined with low atmospheric pressure in the Pacific Ocean, creates a pressure gradient that forces southward winds through the Isthmus of Tehuantepec mountain gap (Figure 1). Those winds reach the Pacific Ocean at the GT with gusts of 35 m/s [*Romero-Centeno et al.*, 2003]. As a comparative example, a tropical storm is upgraded to hurricane status when its sustained winds increase to 33 m/s.

[3] TOPEX/Poseidon (T/P) data and the Naval Research Laboratory (NRL) Layered Ocean Model (NLOM) results show interannual variability in the number and intensity of the Tehuantepec eddies (Figure 2). Assuming that Tehuantepec eddy formation and modulation are predominantly due to the GT winds we would expect to see a GT wind related interannual variability in eddy number and strength. However, the *European Centre for Medium-Range Weather Forecasts* (*ECMWF*) [1994] (Figure 3) and the Fleet Numerical Meteorology and Oceanography Center (FNMOC) Navy Operational Global Atmospheric Prediction System (NOGAPS) [*Rosmond et al.*, 2002] (not shown) wind data sets do not show the hypothesized GT wind related interannual variability in the Tehuantepec eddies. In contrast, NLOM simulations forced with ECMWF and NOGAPS winds show that besides the GT winds (which are the main mechanism for Tehuantepec eddy generation), intraseasonal (30–90 days) and interannual (2–7 years) equatorially generated poleward traveling baroclinic downwelling coastally trapped waves (CTWs) also contribute to the generation and modulation of the Tehuantepec eddies. In similar lines of research, recent studies have discussed and/or invoked the role of CTWs as eddy generators to explain eddy formation in the Gulfs of Alaska and California and in the regions close to Acapulco, Cabo Corrientes, and the María Islands [*Melsom et al.*, 1999; *Murray et al.*, 2001; *Zamudio et al.*, 2002, 2001; L. Zamudio et al., Tropical waves induce oceanic eddies at Cabo Corrientes and the María Islands, Mexico, submitted to *Journal of Geophysical Research*, 2004, hereinafter referred to as Zamudio et al., submitted manuscript, 2004]. Furthermore, W. S. Kessler and Z. Yu (http://www.pmel.noaa.gov/~kessler/t-peckers/phoenix-ams.html, 1998) using an ocean general circulation model noted the

[1]Center for Ocean-Atmospheric Prediction Studies, Florida State University, Tallahassee, Florida, USA.
[2]Naval Research Laboratory, Stennis Space Center, Mississippi, USA.
[3]Department of Marine Sciences, University of Georgia, Athens, Georgia, USA.
[4]Centro de Ciencias de la Atmósfera, Universidad Nacional Autónoma de México, México, D. F.

0148-0227/06/2005JC003182$09.00

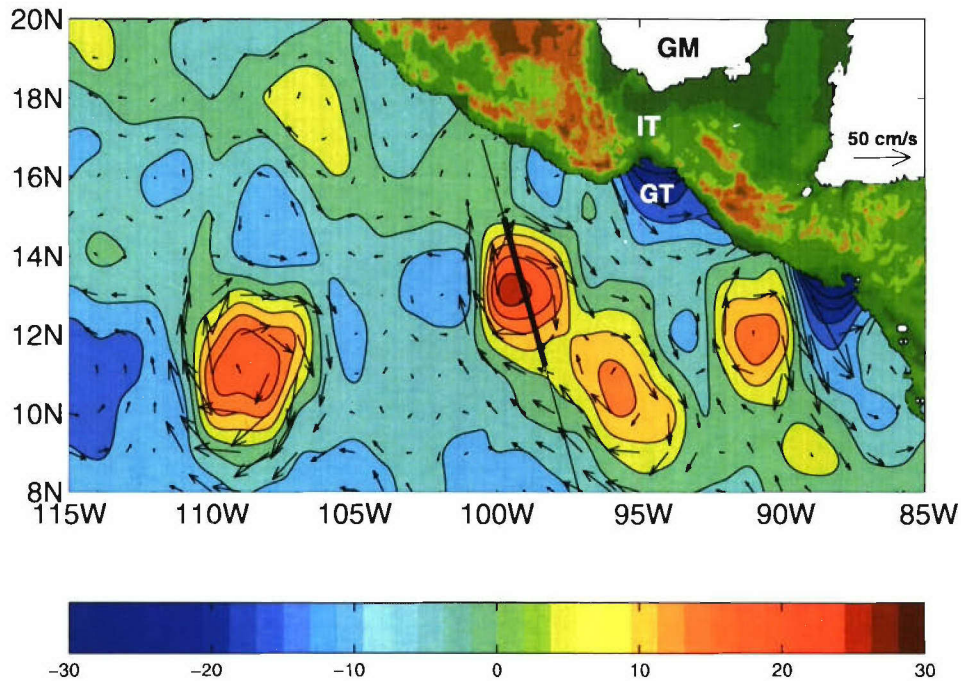

Figure 1. TOPEX/Poseidon (T/P) sea surface height (SSH) anomaly map in centimeters for the period 18–28 February 1993, which shows the presence of anticyclonic Tehuantepec eddies and their associated surface geostrophic circulation (arrow vectors). The map was produced by interpolating all the ascending and descending along-track altimeter measurements to a 1° × 1° regular grid. The anomaly is with respect to the 1993–1999 mean. The positions of the Gulf of Mexico (GM), Isthmus of Tehuantepec (IT), and Gulf of Tehuantepec (GT) are indicated. The bold black line identifies the satellite track along which T/P measured the Tehuantepec eddies shown in Figure 2.

formation of Tehuantepec eddies when GT wind events were absent. On the other hand, *Hansen and Maul* [1991] proposed an alternative generation mechanism for the Tehuantepec eddies that is summarized as the shedding of eddies by the North Equatorial Counter Current during its change of direction around the Costa Rica Dome.

[4] Here we investigate the origin of interannual variability in Tehuantepec eddy generation as measured by satellite altimetry and simulated by a numerical model. Two hypotheses are presented and discussed. The first hypothesis is that the GT winds are the only generator and modulator of the Tehuantepec eddies. The second hypothesis is that in addition to the GT winds, intraseasonal and interannual CTWs also play an important role in Tehuantepec eddy formation and in the modulation of their frequency and amplitude. Hypothesis testing includes assessing the relative importance of GT winds and CTWs in modulating the interannual variability of Tehuantepec eddy generation.

2. Model

[5] The primitive equation formulation of NLOM has been extensively documented by *Hurlburt and Thompson* [1980], *Wallcraft* [1991], *Metzger and Hurlburt* [2001], *Wallcraft et al.* [2003], and Zamudio et al. (submitted manuscript, 2004). NLOM application to Pacific Ocean modeling is discussed by *Hurlburt et al.* [1996]. The main characteristics of the core NLOM experiment used in this study are summarized below. The model consists of 7 layers (including the mixed layer) and includes a free surface, isopycnal outcropping, realistic bottom topography, and coastline geometry that is determined by the 200-m isobath. It is nonlinear, thermodynamic, eddy-resolving (1/16° resolution in latitude by ~0.088° in longitude) and has a domain extending from 20°S to 62°N and from 109.125°E to 77.203°W, but here the focus is on the GT region. The latitudinal extent of the model domain allows study of the effects of equatorially generated signals (i.e., CTWs) in the eastern Pacific Ocean, here specifically on the GT region. The model is forced 1979–2001 with daily averaged heat fluxes and 6-hourly 10-m winds from ECMWF using the methodology of *Kara et al.* [2002] and does not include ocean data assimilation.

3. Results and Discussion

3.1. Tehuantepec Eddies in T/P and NLOM

[6] The T/P satellite altimeter repeats an orbit approximately every 10 days. It measures sea surface height (SSH) every 6.2 km (1 second average) along satellite tracks. The distance between two parallel tracks is about 300 km in our area of study. This wide track separation usually discourages the use of along-track altimeter measurements to track eddies. However, because of the large spatial extent of the long-lived Tehuantepec eddies, which have horizontal dimensions of more than 300 km (Figure 1), and westward propagation speeds of ~11–17 cm/s, the 10-day repeat sampling of T/P depicts their passage and amplitude very clearly in the form of an along-track SSH versus time diagram (positive SSH anomalies in Figure 2).

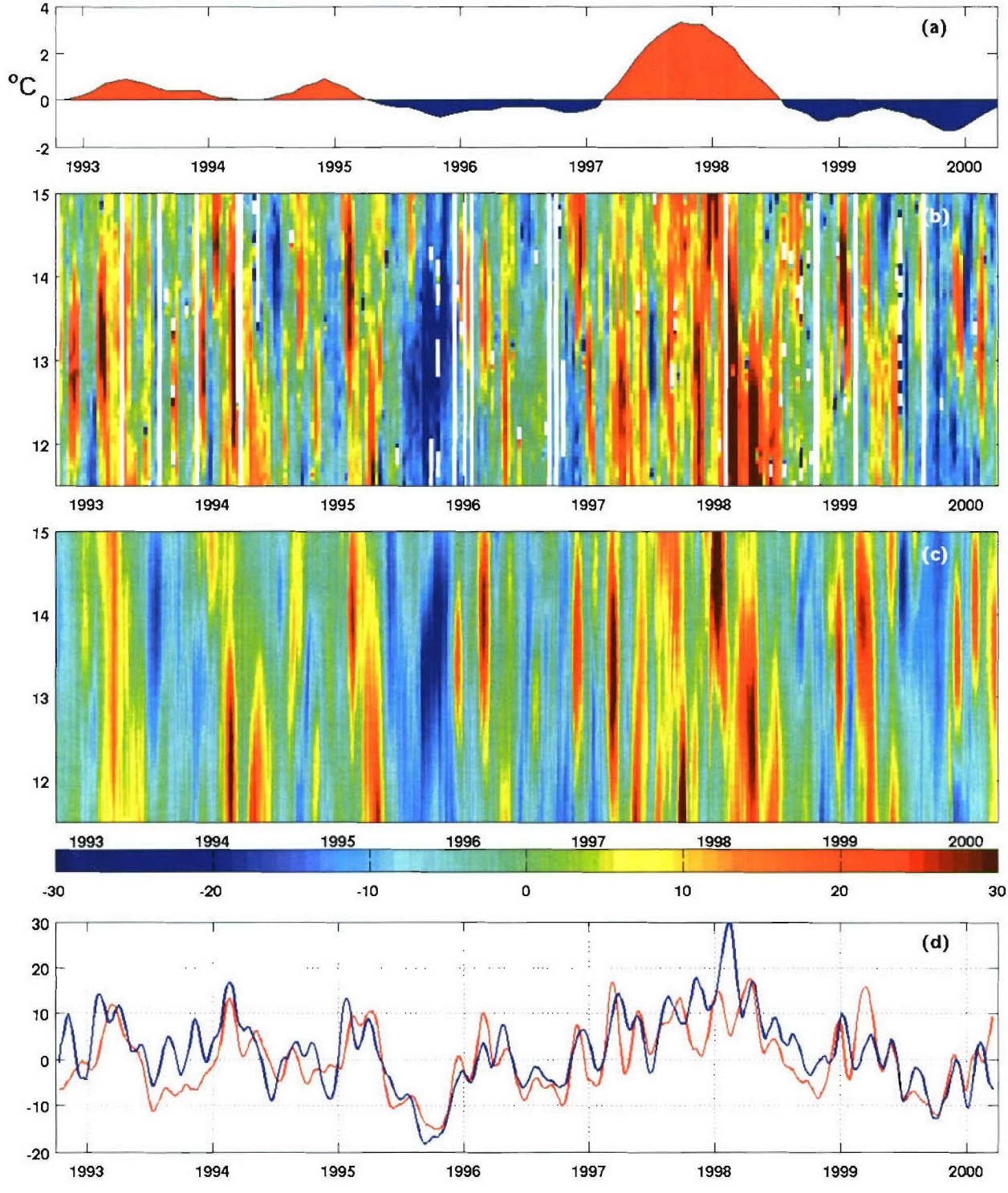

Figure 2. (a) Japanese Meteorological Agency (JMA) El Niño index. Details of the index are given by *JMA* [1991] and ftp://www.coaps.fsu.edu/pub/JMA_SST_Index. The period of study includes the three different scenarios: El Niño (1997), La Niña (1998 and 1999), and neutral years (1992, 1993, 1994, 1995, 1996, and 2000). Sea surface height anomaly time series from (b) TOPEX/Poseidon (T/P) and (c) 1/16° Pacific NLOM. The anomalies are relative to the 1993–1999 mean. Units are centimeters and have been calculated along the bold black segment of the T/P satellite track shown in Figure 1. (d) Latitudinal average of the time series in Figures 2b and 2c. Blue and red lines correspond to T/P and NLOM, respectively. A 1-month running mean filter has been applied to the latitudinally averaged time series. The correlation coefficient between the time series in Figure 2d is 0.72. The first day of each year is labeled.

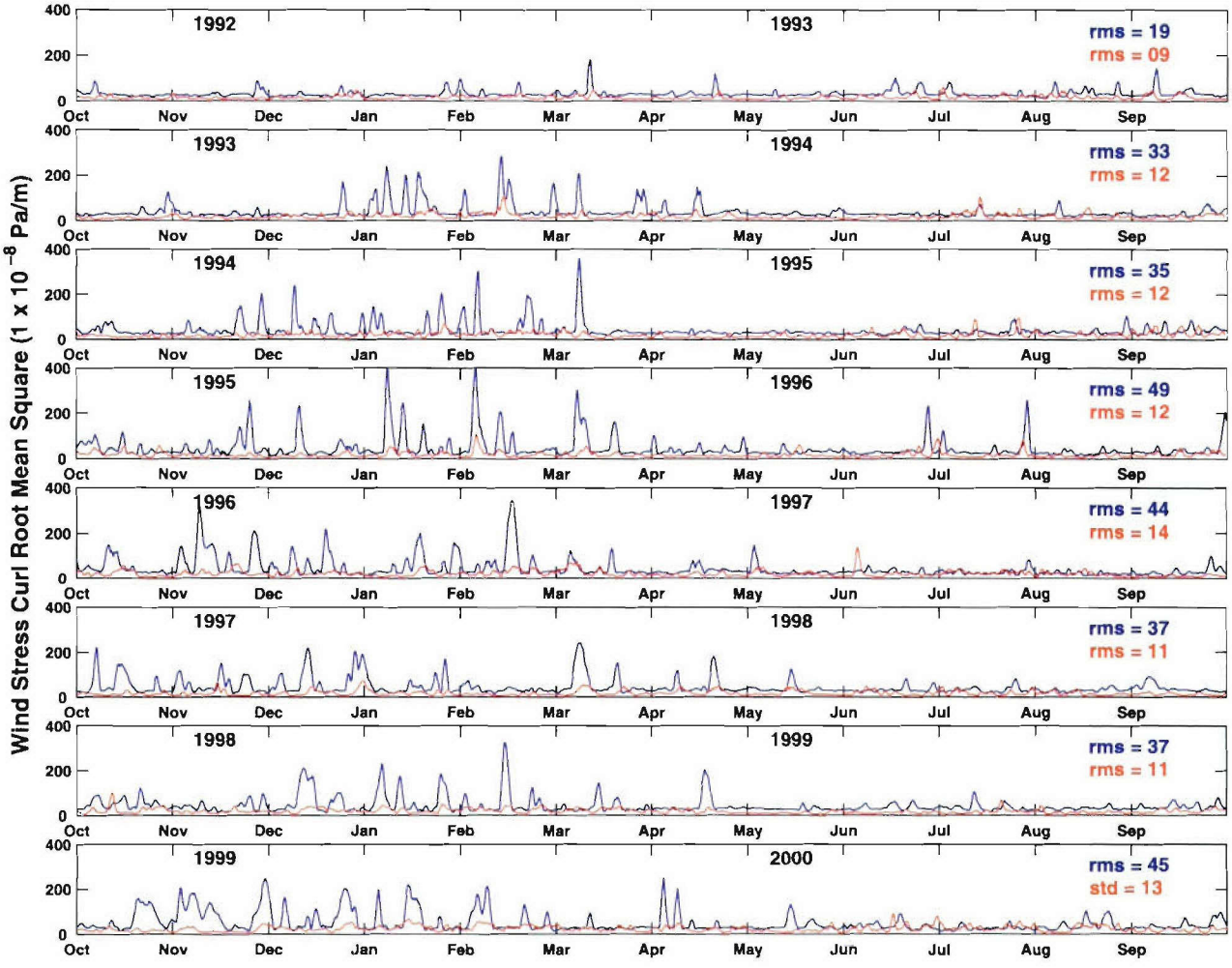

Figure 3. Time series of the European Centre for Medium-Range Weather Forecasts (ECMWF) 10 m wind stress curl (1×10^{-8} Pa/m) root mean square (RMS) difference with respect to the 1979–2001 mean for the Gulf of Tehuantepec and Gulf of Papagayo subregions shown in Figures 6a and 6d, respectively. A 1-day running mean has been applied to the time series. The RMS for each of the eight time series is indicated. The blue and red time series correspond to the Gulf of Tehuantepec and Papagayo, respectively. The first day of each year is labeled.

[7] The T/P and NLOM SSH anomaly data for the period October 1992 to March 2000 (Figures 2b and 2c) show that three to five anticyclonic eddies were formed during each of the first three cold seasons (October–April) (1992–1993, 1993–1994, and 1994–1995). Particularly, the 1992–1993 anticyclonic eddies simulated by NLOM were weaker than those measured by T/P. The 1995–1996 cold season was characterized by the formation of three anticyclonic eddies. Throughout the fall of 1996 no eddies were generated; however, in the 1996–1997 winter season three eddies formed. The T/P and NLOM data suggest the genesis of at least seven anticyclonic Tehuantepec eddies during the 1997–1998 cold season, which was characterized by a strong El Niño event (Figure 2a). Those eddies were characterized by the largest diameter and the highest SSH anomaly. A peculiar characteristic of 1997 is that the eddy generation continued for the entire year in both T/P and NLOM. The 1998–1999 cold season T/P data record includes just two anticyclonic eddies and three during the 1999–2000 cold season. During these last two cold seasons a La Niña event was taking place in the Pacific Ocean (Figure 2a). Table 1 summaries the number of Tehuantepec eddies measured by T/P and simulated by NLOM during the 8 cool seasons (October–April) and 7 warm seasons (May–September) analyzed in this study.

[8] It is remarkable how the model (which does not include ocean data assimilation) reproduces most of the Tehuantepec eddy characteristics measured by T/P. Indeed, the correlation coefficient between the latitudinally averaged observed (T/P) and simulated (NLOM) time series is 0.72, suggesting a semideterministic nature for the generation and evolution of Tehuantepec eddies (Figure 2d).

[9] The SSH time series in Figure 2 show Tehuantepec eddy formation during the entire year of 1997, even when strong Tehuantepec wind events do not occur (Figure 3). This suggests the existence of an alternative generation mechanism for Tehuantepec eddies, and advantages of using SSH satellite altimeter data instead of satellite sea surface temperature (SST) data for the study of the Tehuantepec eddies. CTWs are presented as the alternate mechanism, a topic discussed in section 3.3. The warm-core anticyclonic Tehuantepec eddies exist in a region where

Table 1. Number of Anticyclonic Tehuantepec Eddies Measured by T/P and Simulated by NLOM During the Eight Cool Seasons (October–April) and Seven Warm Seasons (May–September) Analyzed in This Study[a]

Cool Season			Warm Season				
Year	Number of Eddies in T/P	Number of Eddies in NLOM	Year	Number of Eddies in T/P	Number of Eddies in NLOM	Total in T/P	Total in NLOM
1992–1993	3	3	1993	1	1	4	4
1993–1994	4	3	1994	1	1	5	4
1994–1995	5	4	1995	1	0	6	4
1995–1996	3	3	1996	0	1	3	4
1996–1997	3	3	1997	2	2	5	5
1997–1998	7	7	1998	1	1	8	8
1998–1999	2	3	1999	2	1	4	4
1999–2000	3	3					

[a]The total number of anticyclonic eddies, in T/P and NLOM, includes the eddies in a cool season plus the eddies in the following warm season.

the surrounding water is also warm [*Hansen and Maul*, 1991]. However, during their formation and for a few days after, the anticyclonic Tehuantepec eddies are clearly recognized in satellite SST images (Figure 4). This is enhanced by the strong SST gradient, which is created by the large mixing and upwelling induced SST decrease along the axis of the GT wind path. Conditions like those shown in Figure 4 last only a few days since they are generated by the temporary strong wind events. When the eddies propagate to the west the eddy thermal signature is difficult to discern in satellite SST images because, once the strong cooling ceases, the eddy air-sea temperature differences stimulate large heat fluxes in the tropics that reduce the strong SST gradient and eventually render the eddies undetectable in thermal images. Therefore satellite altimeter SSH observations can be more useful for the study of eddies in this tropical ocean.

3.2. GT Wind as the Generator and Modulator of Tehuantepec Eddies

[10] An index of the El Niño – La Niña signal (Figure 2a) and the SSH anomaly time series (Figures 2b–2d) indicate that the seasons characterized by the fewest and the smallest Tehuantepec eddies (1995–1996, 1998–1999, and 1999–2000) coincided with the cold phase of the index. Whereas the seasons characterized by the largest (number, diameter and SSH anomaly) Tehuantepec eddies (1992–1993, 1993–1994, 1994–1995, and 1997–1998) occurred during the warm phase. One explanation for this modulation of Tehuantepec eddies is as follows. Given the results in Figure 2 and assuming that the GT winds are the only mechanism for generation and modulation of Tehuantepec eddies, then fewer and/or weak Tehuantepec eddies would be caused by fewer and/or weaker GT wind events. This could occur as a result of weak atmospheric pressure gradients between the Gulf of Mexico and the Pacific Ocean and weaker and/or less frequent cold fronts passing through the Gulf of Mexico. The anomalous location of the jet stream, which is shifted southward (northward) during the warm (cold) phase of the index strengthening (weakening) the cold fronts that reach the Gulf of Mexico [*Quadrelli and Wallace*, 2002], is consistent with Tehuantepec eddy interannual variability measured by T/P (Figure 2b), simulated by NLOM (Figure 2c) and with the preceding explanation.

[11] To test this hypothesis we analyzed 1979–2001 ECMWF 6-hourly 10-m winds, 1979–2001 ECMWF 12-hourly 1000 mb winds and 1990–2001 NOGAPS 6-hourly surface stresses over the GT region. An example for the ECMWF 10-m winds over the period October 1992 to September 2000 is shown in Figure 3. The analyses show that the ECMWF and NOGAPS winds reproduce several satellite scatterometer and in situ measured features of the GT winds [*Bourassa et al.*, 1999; *Chelton et al.*, 2000a, 2000b; *Romero-Centeno et al.*, 2003] (http://www.coaps.fsu.edu/qscat/anim). Those characteristics are strong wind events mainly during fall–winter, a wind event duration of ~2–3 days, and wind speed and negative (positive) wind stress curl on the west (east) side of the wind path. Furthermore, *Kelly et al.* [1999] performed an exhaustive model/data comparison between ECMWF winds and the NASA scatterometer (NSCAT) winds in the tropics, including the Tehuantepec and Central America regions, which shows the capability of ECMWF to accurately represent the winds of the region. Even though the different wind products realistically represent the GT winds, the statistics (the root mean square of the wind stress curl) do not show

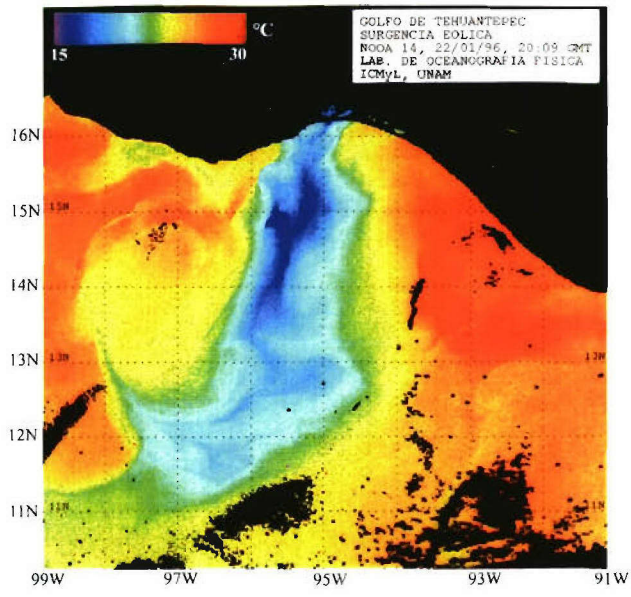

Figure 4. Sea surface temperature (°C) in the Gulf of Tehuantepec region as measured by the NOAA 14 satellite on 22 January 1996. Image processed by Agustin Fernandez (Universidad Nacional Autónoma de México). It shows upwelling and mixing (cold SST) and an anticyclonic eddy driven by a Tehuantepec wind event.

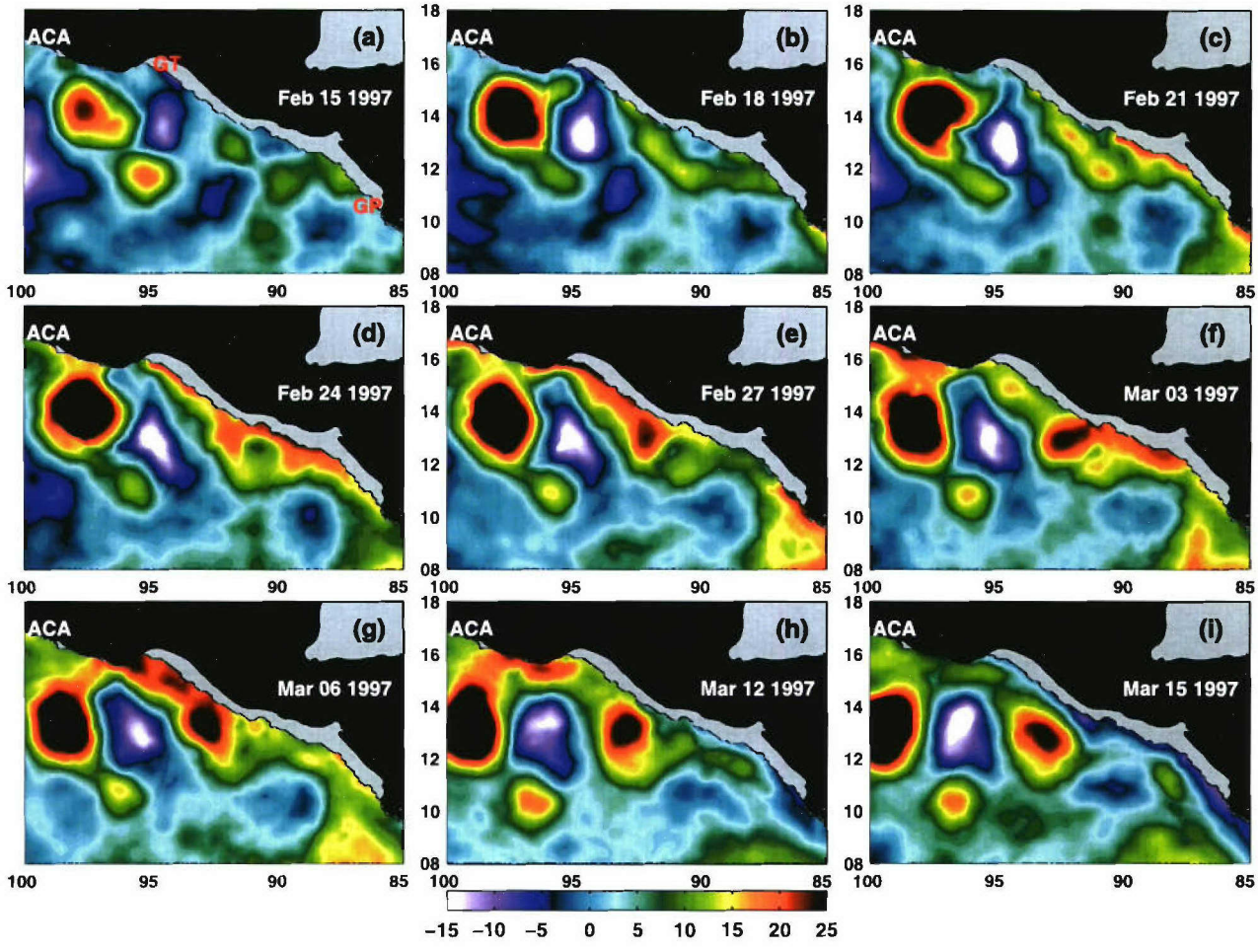

Figure 5. Sea surface height anomaly (color contours in centimeters) for nine different dates in February–March 1997 as simulated by 1/16° Pacific NLOM forced by ECMWF 6 hourly 10 m winds and daily averages for the other fields used in the thermal forcing. The locations of the Gulf of Papagayo (GP), Gulf of Tehuantepec (GT), and Acapulco (ACA) are indicated. The gray area represents ocean areas not modeled by Pacific NLOM, i.e., depths shallower than 200 m.

significant interannual variability (Figure 3). In addition, a visual inspection of the time series in Figure 3 does not indicate important differences in the number and intensity of the wind events during the two opposite cool season regimes, the 1997–1998 (El Niño year) and 1999–2000 (La Niña year). Note also that during 1997 the Tehuantepec eddy generation extends beyond the 1996–1997 cold season. That fact cannot be explained in terms of wind stress curl alone, because the wind stress curl in spring-summer is significantly weaker than in fall-winter (Figure 3). Hence the lack of interannual variability in the wind fields suggests that by themselves the GT winds are not sufficient to explain the satellite measured Tehuantepec eddy interannual variability.

3.3. Coastally Trapped Waves and the Tehuantepec Eddies

3.3.1. Coastally Trapped Waves and Winds

[12] A sequence of snapshots showing the GT winds and the CTW as modulators and generators of Tehuantepec eddies are presented in Figures 5 and 6. On 15 February 1997 the SSH anomaly around the GT is characterized by two anticyclonic eddies and one cyclonic eddy (Figure 5a). The anticyclones have maximum SSH anomalies of ~15 and 20 cm and centers close to 95°W, 11.8°N and 97.5°W, 14°N, respectively. The cyclonic eddy has minimum SSH anomaly of ~−11 cm at its center (94.5°W, 13.6°N). The three eddies were generated by the wind events that occurred in the GT during January 1997 (Figure 3). In addition, Figure 5a shows areas of positive SSH anomaly around 90°W, 12°N. The wind stress curl is strong and anticyclonic (cyclonic) on the western (eastern) side of the GT (Figure 6a). This wind stress curl strengthened the larger anticyclonic eddy and the cyclonic eddy, increasing the amplitude of the SSH anomalies to a maximum >25 cm and a minimum <−15 cm, respectively (Figures 5b). In addition, the tip of a downwelling CTW is entering the region near 85°W, 10°N and there is weak wind stress curl in the entire study area, except for the GT, as can be seen in Figures 5b and 6b. Next, the wind stress curl weakened considerably, the CTW propagated northward, and a new anticyclonic eddy formed on the southeast side of the GT (92.5°W, 12.5°N) (Figures 5c–5g and 6c–6g). Note that in spite of the weak anticyclonic wind stress curl to the southeast of the GT, which is ~7 times smaller than to the west of the GT (Figure 6), an anticyclonic eddy was

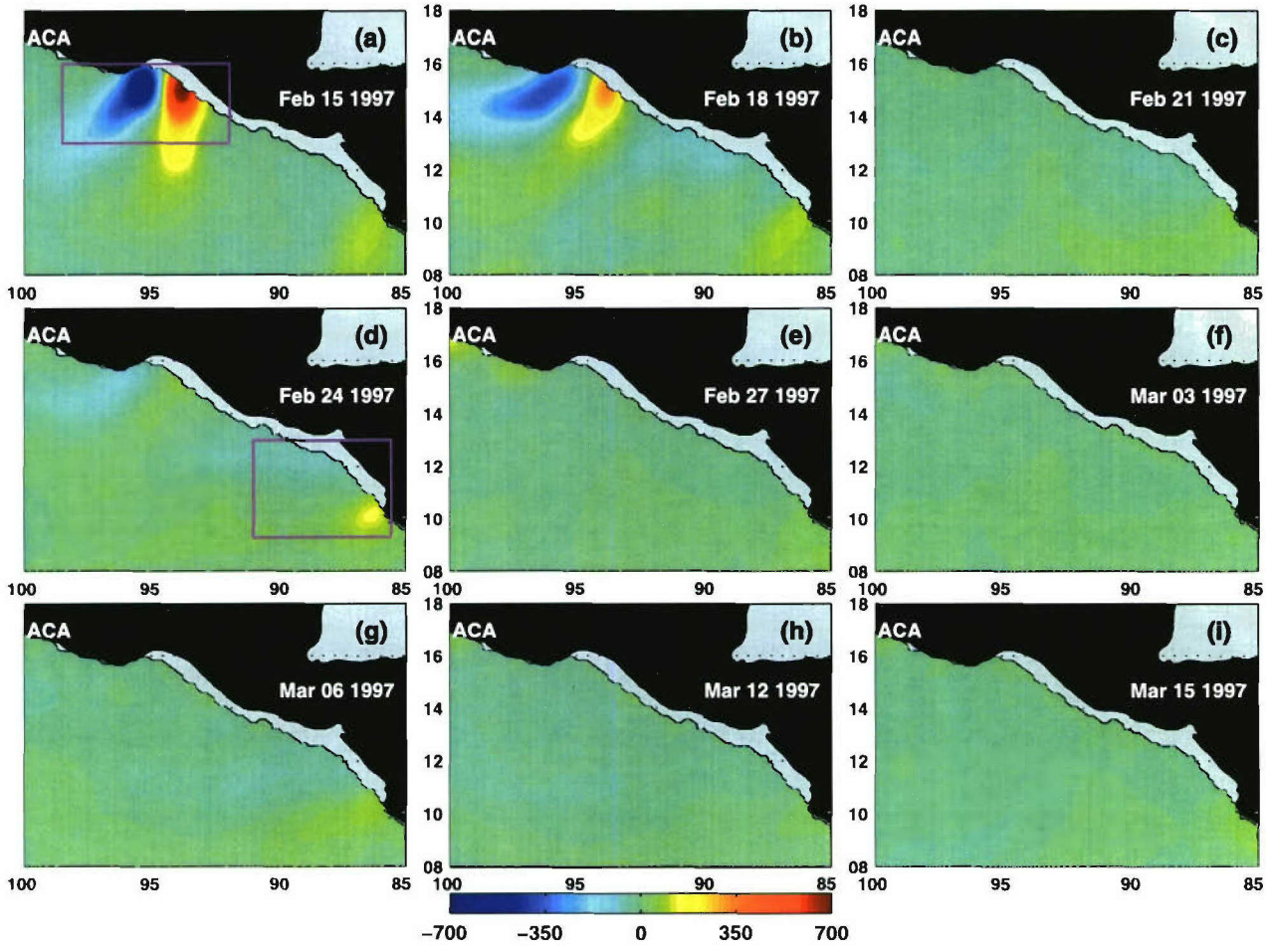

Figure 6. Wind stress curl (color contours in 1×10^{-8} Pa/m) for nine different dates in February–March 1997 as determined from the ECMWF 10-m winds. The magenta boxes in Figures 6a and 6d indicate the two areas where the time series of Figure 3 were extracted.

generated in this region (Figure 5). Finally, the tail of the CTW reached and crossed the Acapulco region and the area of study was populated with larger and stronger eddies than a month prior (Figures 5h–5i).

[13] It is noteworthy that the GT winds strengthened the anticyclonic (cyclonic) eddy located on the western (central-eastern) side of the GT on 15 February 1997 (Figures 5 and 6). That is an example of the GT winds as a generator and modulator of the Tehuantepec eddies. However, equally notable is the formation of the anticyclonic eddy to the southeast of the GT that coincides with the passage of the CTW through the area during a period of weak anticyclonic wind stress curl (Figures 5c–5g and 6c–6g). Hence some questions present themselves. What is the origin of these downwelling CTWs? How do they fluctuate interannually? How do the CTWs contribute to the modulation/formation of the Tehuantepec eddies?

[14] During the boreal fall/winter season the equatorial Pacific is characterized by the formation of 2–4 intraseasonal (30–90 day) baroclinic downwelling Kelvin waves, which are more (less) common and more intense (weaker) during El Niño (La Niña) years. These waves propagate eastward until they reach the west coast of the Americas, where they split into northward and southward propagating CTWs with the northward CTWs reaching the GT and beyond [*Spillane et al.*, 1987; *Enfield*, 1987; *Kessler et al.*, 1995; *Melsom et al.*, 2003]. Figure 7 is a diagram of along equatorial and along coastal SSH versus time, as simulated by NLOM. It shows (1) the western and central Pacific as the generation region for the equatorial waves, (2) a nearly constant propagation speed (~2.3 m/s) for the waves, which denotes their nondispersive character, (3) interannual variability in both number and strength of the waves, (4) proliferation of the waves during the boreal cold season and during El Niño events, and (5) wave amplification as the waves propagate poleward along the coast.

[15] Considering that both the intraseasonal baroclinic downwelling CTWs and the Tehuantepec winds are distinctive features of the eastern tropical Pacific, which are maximal during the boreal cool season, the oceanic effects of both may coincide in space and time around the GT. The Tehuantepec winds, which inject large amounts of energy into the GT waters (Figure 8a), induce negative (positive) relative vorticity on the western (central-eastern) side of the GT (Figure 8b) via Ekman pumping (suction). In the process a strong converging (diverging) Ekman transport increases (decreases) the oceanic pressure (Figure 8c) and in

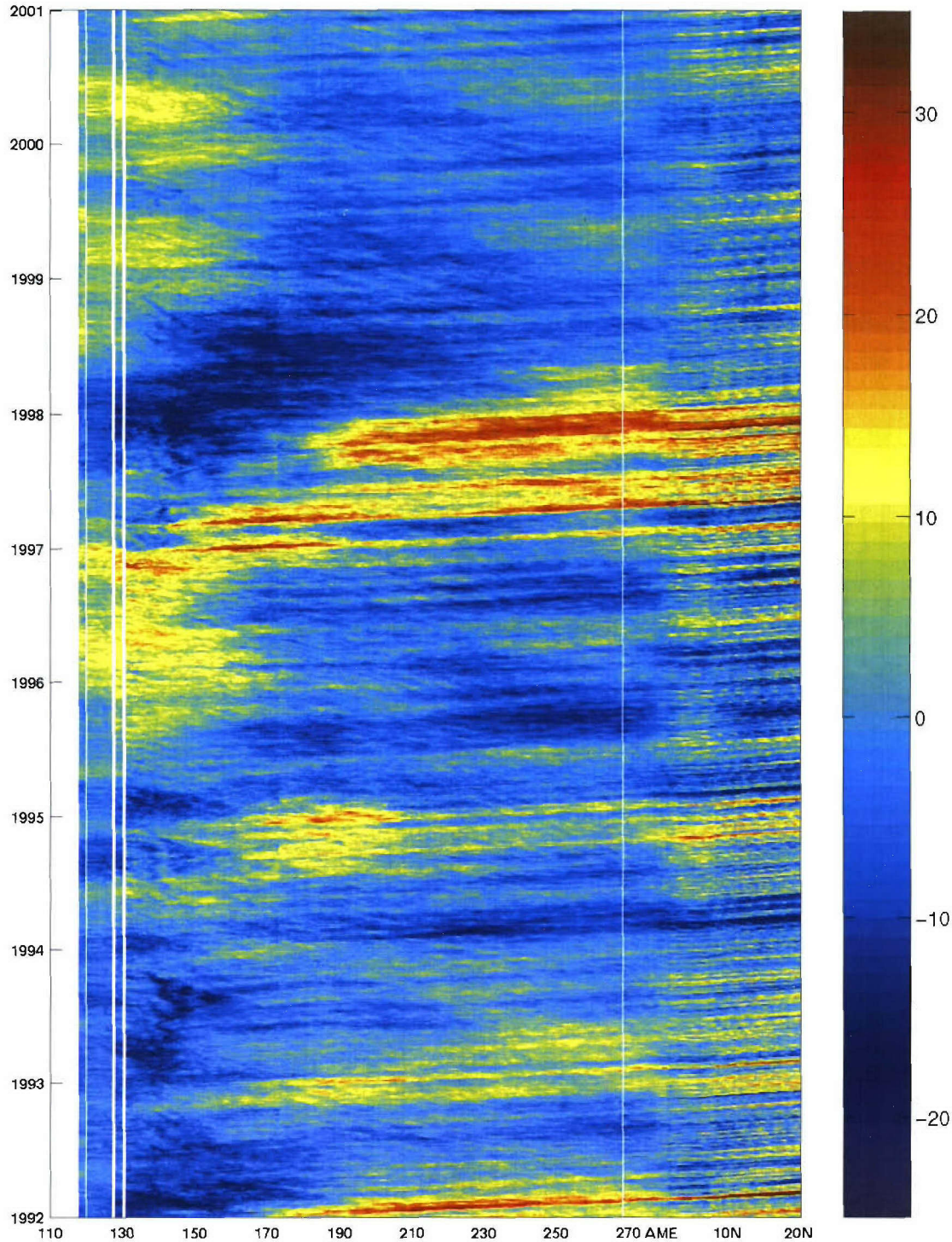

Figure 7. Sea surface height anomaly (color contours in centimeters) time series from 1/16° Pacific NLOM, first along the equator (starting in the western Pacific and propagating eastward until arrival at the Americas West Coast), and second along the coast to the 20°N. The white vertical lines to the west of 130°E indicate the location of Equatorial Western Pacific Islands and the white vertical line close to 270°E indicates the location of the Galapagos Islands. The equatorial position of the Americas West Coast is indicated by AME. The first day of each year is labeled.

the convergence (divergence) areas, lowers (raises) the thermocline (Figure 8d), increases (decreases) the SSH (Figure 8e), decreases (increases) potential vorticity (Figure 8f), and forms anticyclonic (cyclonic) eddies (Figure 8). At the same time, the northward propagating baroclinic downwelling CTW induces strong poleward currents as it passes (Figure 9), increasing the energy along the coast (Figure 8a). Also, this wave increases the coastal

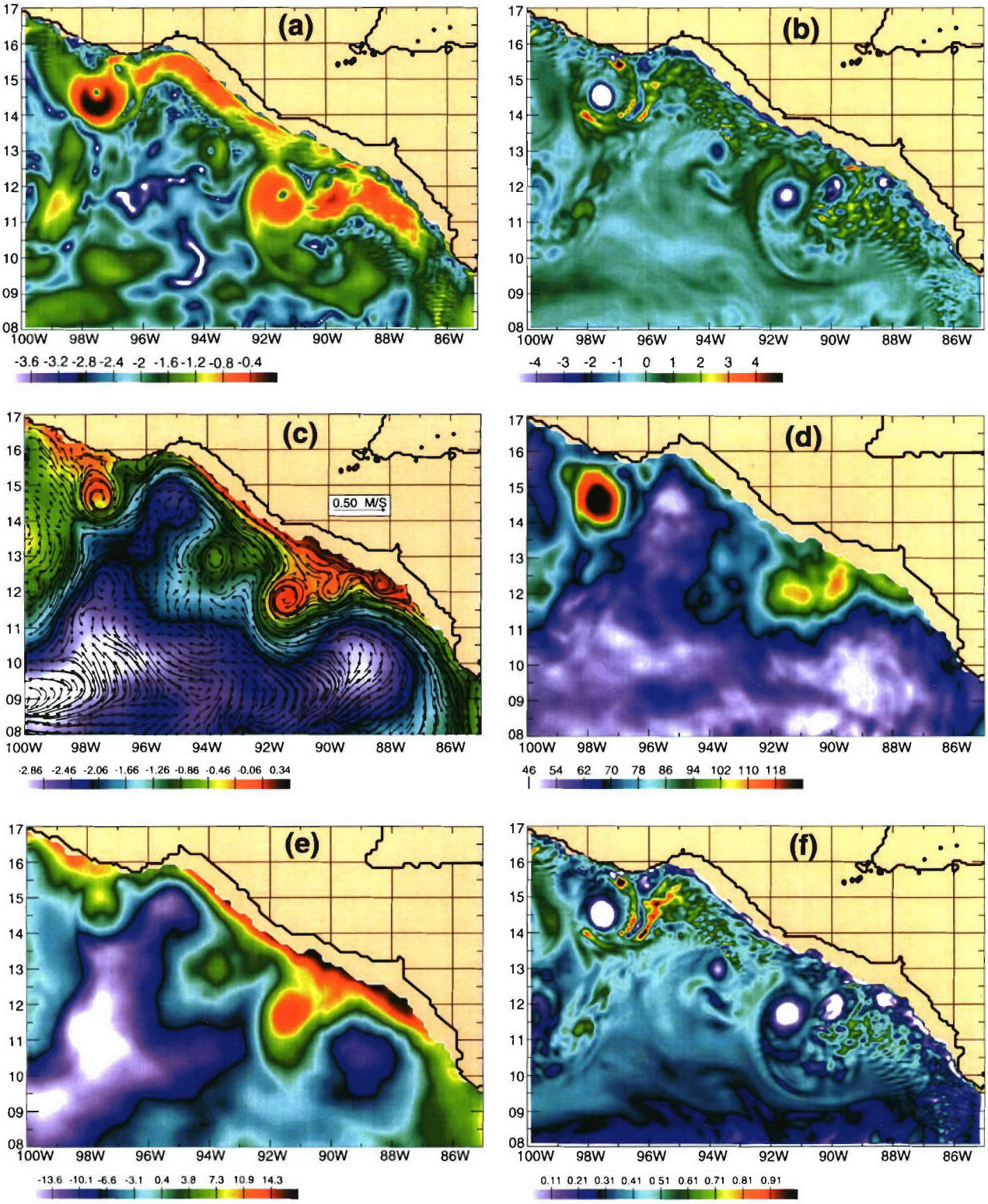

Figure 8. Snapshots for 1 January 1997 as simulated by 1/16° Pacific NLOM. (a) Surface kinetic energy anomaly per mass (color contours in log (m^2/s^2)), (b) surface relative vorticity anomaly (color contours in 1×10^{-5} s^{-1}), (c) density normalized surface pressure anomaly (color contours in m^2/s^2) and currents (arrow vectors), (d) surface layer thickness (color contours in meters), (e) sea surface height (color contour in centimeters), and (f) surface potential vorticity anomaly (color contours in 1×10^{-6} m^{-1} s^{-1}).

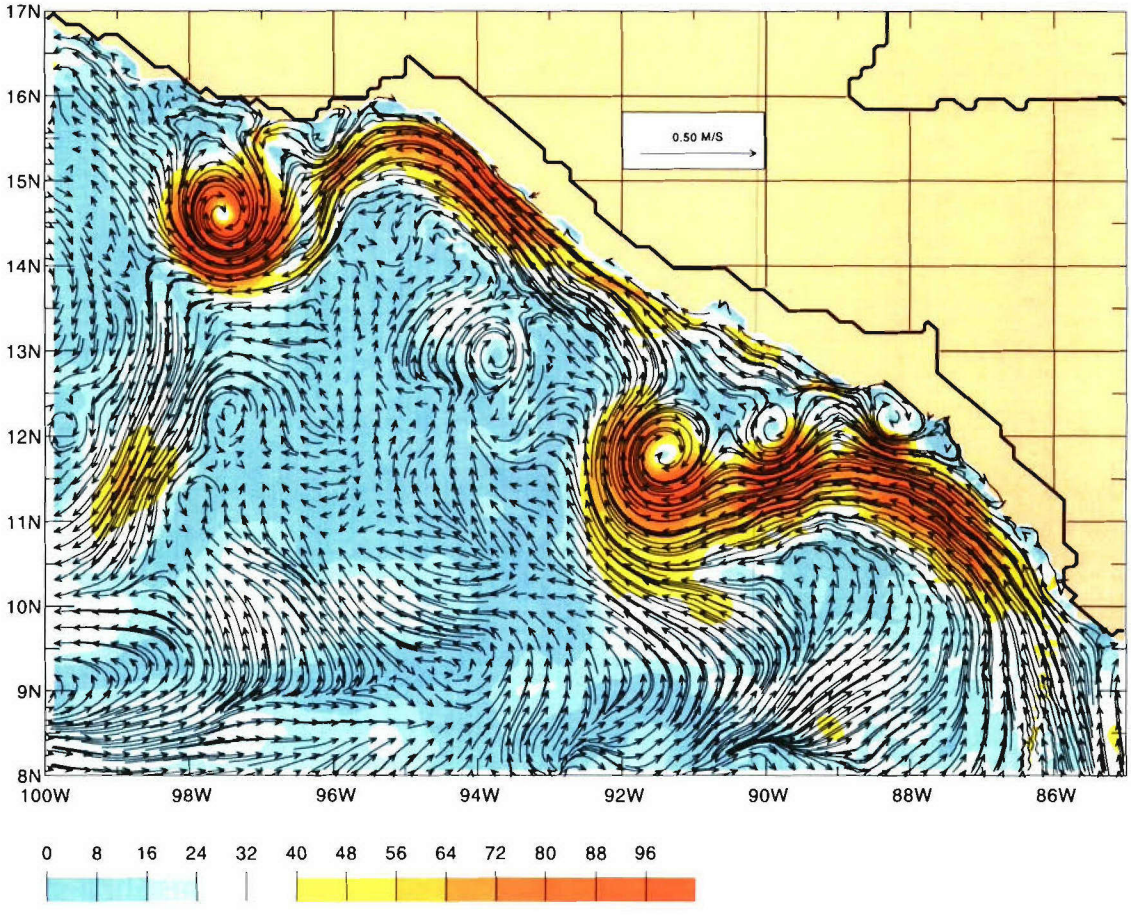

Figure 9. Surface currents (arrow vectors) and current speed (color contours in cm/s) for 1 January 1997 as simulated by 1/16° Pacific NLOM.

SSH (Figure 8e), increases the coastal pressure (Figure 8c), and depresses the coastal thermocline (Figure 8d). Furthermore, the currents induced by the CTW produce a strong horizontal shear flow that is a source of negative (positive) relative vorticity in the inshore (offshore) oceanic regions during the passage of the wave (Figures 8b and 9). This extra negative relative vorticity is restricted to the lateral frictional boundary layer, which has an offshore extension of ~10 km and is several times smaller than the radius of the anticyclonic eddies (>100 km) (Figures 8 and 9). Hence this extra negative relative vorticity is probably not responsible for initiating the formation of the eddies. In addition, the northward propagating downwelling CTW can be a source of low values of potential vorticity for the GT region. As an example, note the similarity between the potential vorticity values in the equatorial Pacific and the potential vorticity values along the coast, which are associated with the passage of the CTW through the region, and the potential vorticity values of the anticyclonic eddies (Figure 10). How do intraseasonal baroclinic CTWs influence on the generation of the eddies? This question is addressed in the next section.

3.3.2. Intraseasonal CTWs and Eddy Generation

[16] According to linear equatorial wave theory, for a given frequency there exists a critical latitude below which unforced CTWs radiate energy offshore in the form of long Rossby waves [*Clarke and Shi*, 1991]. Considering that for intraseasonal frequencies (30–90 days) the nonmeridional coasts of Central America and southwest Mexico are located to the north of the critical latitude [*Clarke and Shi*, 1991, Table 1], then the free propagating intraseasonal CTWs of Figures 5, 7, and 8 will not separate from the coast. Consequently the formation of eddies via CTW detachment from the coasts of Central America and southwest Mexico is not a mechanism that will occur during the passage of intraseasonal CTWs. Also, for the particular case of the anticyclonic eddy centered near 92.5°W, 13.2°N in Figure 5f, the wind as the eddy generator can be dismissed, since this eddy formed during a period of weak winds (Figure 6). Then, what was the generation mechanism for this eddy?

[17] The CTWs discussed here are generated by equatorial winds. Thus they could be surface intensified and characterized by a vertical shear flow (Figures 5, 9, and 11), making them candidates for triggering baroclinic instability. Also, CTWs induce strong surface currents in the areas of their passage, generating a strong horizontal shear flow (Figures 5, 9, and 11), making them a candidate for triggering barotropic instability. Thus we hypothesize that Tehuantepec eddies can be modulated and/or generated by barotropic and/or baroclinic instabilities, which are triggered by CTWs.

[18] Baroclinic instabilities occur when perturbations grow by drawing energy from the available potential energy

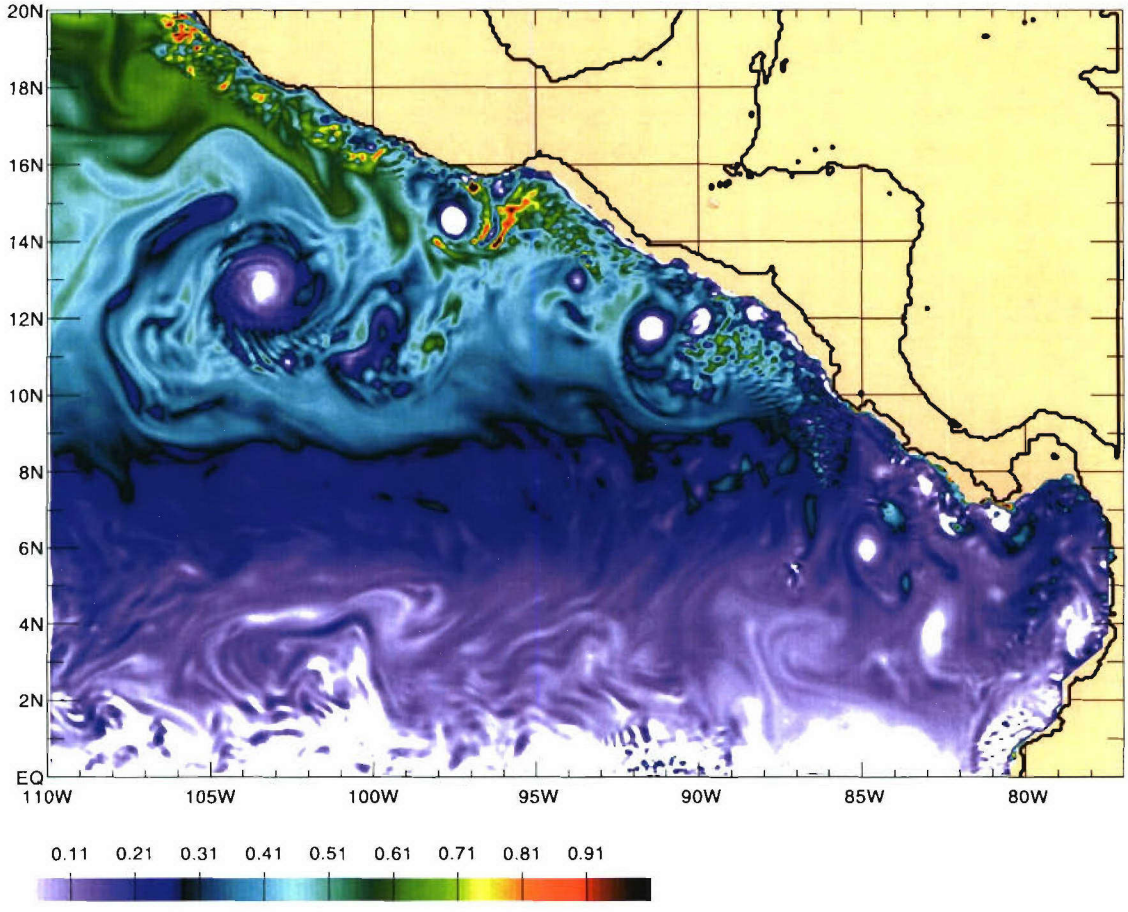

Figure 10. Surface potential vorticity anomaly (color contours in 1×10^{-6} m^{-1} s^{-1}) for 1 January 1997 as simulated by 1/16° Pacific NLOM.

associated with sloping isopycnals [*Kundu*, 1990]. In the case of baroclinic downwelling CTWs these are characterized by a sharp rise of the SSH toward the coast (Figures 5b–5i). *Spall* [1992] proposed and calculated baroclinic instabilities in the southwestward eastern boundary current known as the Cape Verde Frontal Zone as a means to generate radiating baroclinic Rossby waves, which produce mesoscale variability in the mid-ocean. In the GT case the current is a northwestward eastern boundary current, which is associated with the passage of poleward propagating baroclinic downwelling CTWs that could trigger the development of barotropic and baroclinic instabilities, which in turn could trigger the development of eddies and related mesoscale variability. Thus we search for signatures of barotropic and baroclinic instabilities in the pressure, energy (section 3.3.3) and currents fields, and we isolate the effects of baroclinic instabilities analyzing the results of a 1.5-layer reduced gravity simulation (section 3.3.3).

[19] Some support for the hypothesis of baroclinic instabilities as a trigger for development of Tehuantepec eddies is provided by the vertical structure of the eddies. As an example of that, the surface layer pressure overlain on the fifth layer pressure (Figure 12) shows a significant phase difference between the two layers in the vicinity of the eddy centered near 93°W, 13.2°N. This is a signature of baroclinic instability when it occurs during a period of rapid eddy intensification, but can occur for any propagating baroclinic eddy because of the pattern of vortex stretching and compression [e.g., see *Hurlburt et al.*, 1990].

[20] What is the role of barotropic instabilities in the development of the Tehuantepec eddies? Was the new eddy in Figure 5 triggered by barotropic instabilities? Barotropic instabilities are due to perturbations where the energy is supplied by the horizontal shear of the currents. To provide some insight into the origin of the instabilities generated by the CTW in Figure 5, a Beta Rossby number, which is defined as the ratio of relative to planetary vorticity advection, $R_B = \upsilon/\beta r^2$, was calculated. Here υ is the maximum swirl velocity of an eddy averaged around the eddy, and r is the mean radius of the eddy at υ. R_B of order 1 (10) suggests barotropic (baroclinic) instabilities involving the first baroclinic (barotropic) mode [*McWilliams and Flierl*, 1979; *Hurlburt and Thompson*, 1982, 1984; *Murphy et al.*, 1999]. In the case of the eddy with center close to 93°W, 13.2°N on 12 March 1997 (Figure 5h) $\beta \approx 2.2 \times 10^{-11}$ m^{-1} s^{-1}, υ = 50 cm/s and $r \approx 100$ km. Consequently, $R_B \approx 2.3$ suggesting a key role for barotropic or internal mode baroclinic instabilities [*Hurlburt et al.*, 1996] in the formation of this particular eddy.

[21] Taken together, the results in Figures 5, 6, and 11–12 show signatures consistent with barotropic and baroclinic instabilities triggered by a short-wavelength intraseasonal baroclinic downwelling CTW during a period of weak GT winds, and the possible influence of the instabilities on the

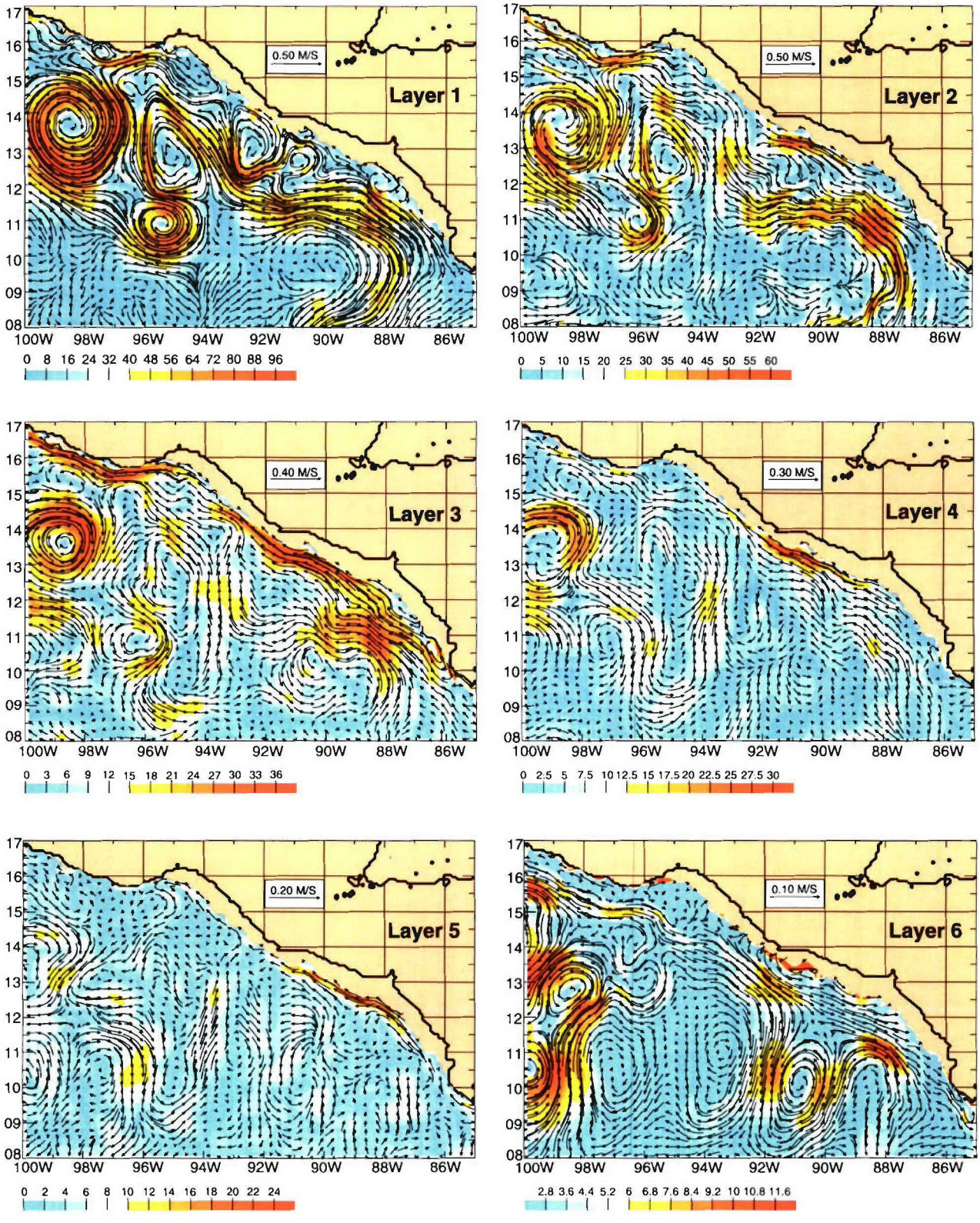

Figure 11. Currents (arrow vectors) and current speed (color contours in cm/s) for six layers on 3 March 1997 as determined by 1/16° Pacific NLOM.

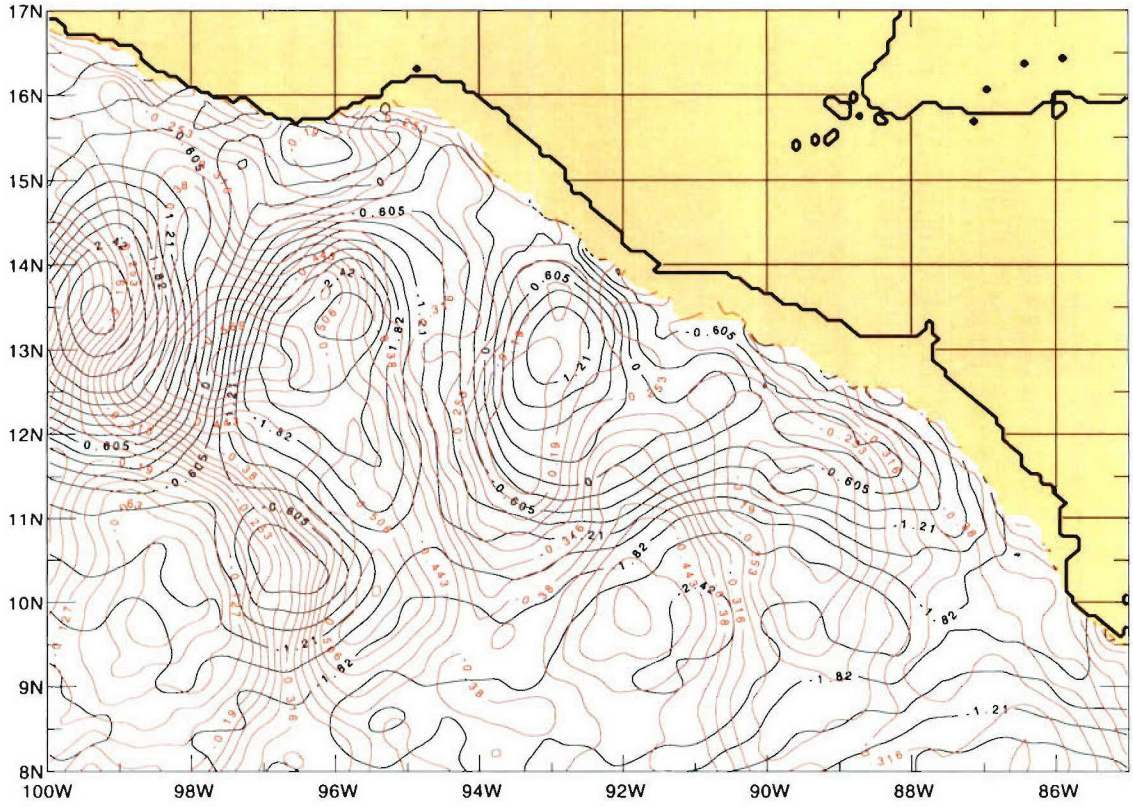

Figure 12. Surface layer pressure (red in m^2/s^2) overlain on layer 5 pressure (black in m^2/s^2) for 12 March 1997 as simulated by 1/16° Pacific NLOM. Note the phase lag in the vicinity of the eddy centered near 93°W, 13.2°N.

development of an anticyclonic eddy southeast of the GT. Since this new mechanism for generation of Tehuantepec eddies is not wind dependent, then it should be possible to isolate its effects during summer time, when strong offshore GT wind events are rare (Figure 3).

3.3.3. Tehuantepec Eddy Generation During the Summer of 1997

[22] To provide additional insight concerning CTW impact on Tehuantepec eddy formation, we document the generation of two anticyclonic eddies during the summer of 1997. These occur during a 5-month period (mid-May to early October) of weak GT and Papagayo winds (Figure 3). Detailed discussion of the Papagayo winds is given by *Schultz et al.* [1997, and references therein] and *Chelton et al.* [2000a, 2000b, and references therein]. On 14 June 1997 the SSH anomaly field along the coast from Central America to the entrance of the Gulf of California was characterized by generally weak highs and lows in SSH, generally weak cyclonic and anticyclonic eddies, a lack of anticyclonic eddies in the GT area, and by only a weak CTW (Figure 13a). However, two weeks later the tip of an arriving downwelling CTW (positive SSH anomaly of ~20 cm) can be seen along the Central America coast (85°W, 10°N) in Figure 13b. This long-wavelength (i.e., south of the critical latitude) CTW (which is associated with the 1997 El Niño event) continued propagating northward and raising the coastal region SSH from Central America to the entrance of the Gulf of California (Figures 13b–13g). According to the linear equatorial wave theory for interannual frequencies, the nonmeridional coasts of Central America and southwest Mexico are located to the south of the critical latitude [*Clarke and Shi*, 1991, Table 1]. Hence, during its northward propagation the interannual CTW radiates energy westward in the form of Rossby waves (Figure 13). The simultaneous occurrence of these two processes, the northward propagation of the CTW and its westward radiation of energy, can be recognized by noting the narrow cross-shore trapping scale of the CTW (which is proportional to the radius of deformation) (Figures 13b–13g) and the subsequent westward propagation of this positive SSH anomaly. By 17 August 1997 it is completely separated from the coast (Figures 13h–13r). Also, note that on 18 July 1997 a short-wavelength baroclinic downwelling CTW (which is characterized by a SSH anomaly of ~30 cm) reached the area of study and its passage through the GT region coincided with the formation of anticyclonic Tehuantepec eddies on the southeast (90°W, 12.7°N) and northwest (96.5°W, 15.5°N) sides of the GT (Figure 13h–13n). Since these two eddies were formed during the 5-month period of weak GT and Papagayo winds during 1997 (Figure 3), the wind can be dismissed as the source of energy for the generation of the eddies. Then, what is the generation mechanism for these eddies? Did the CTWs in Figure 13 trigger barotropic and/or baroclinic instabilities?

[23] The propagation of the two CTWs along the coasts of Central America and southwest Mexico is illustrated by the thickness of the two top model layers (Figure 14). The coastal deepening effects of the long-wavelength CTW are

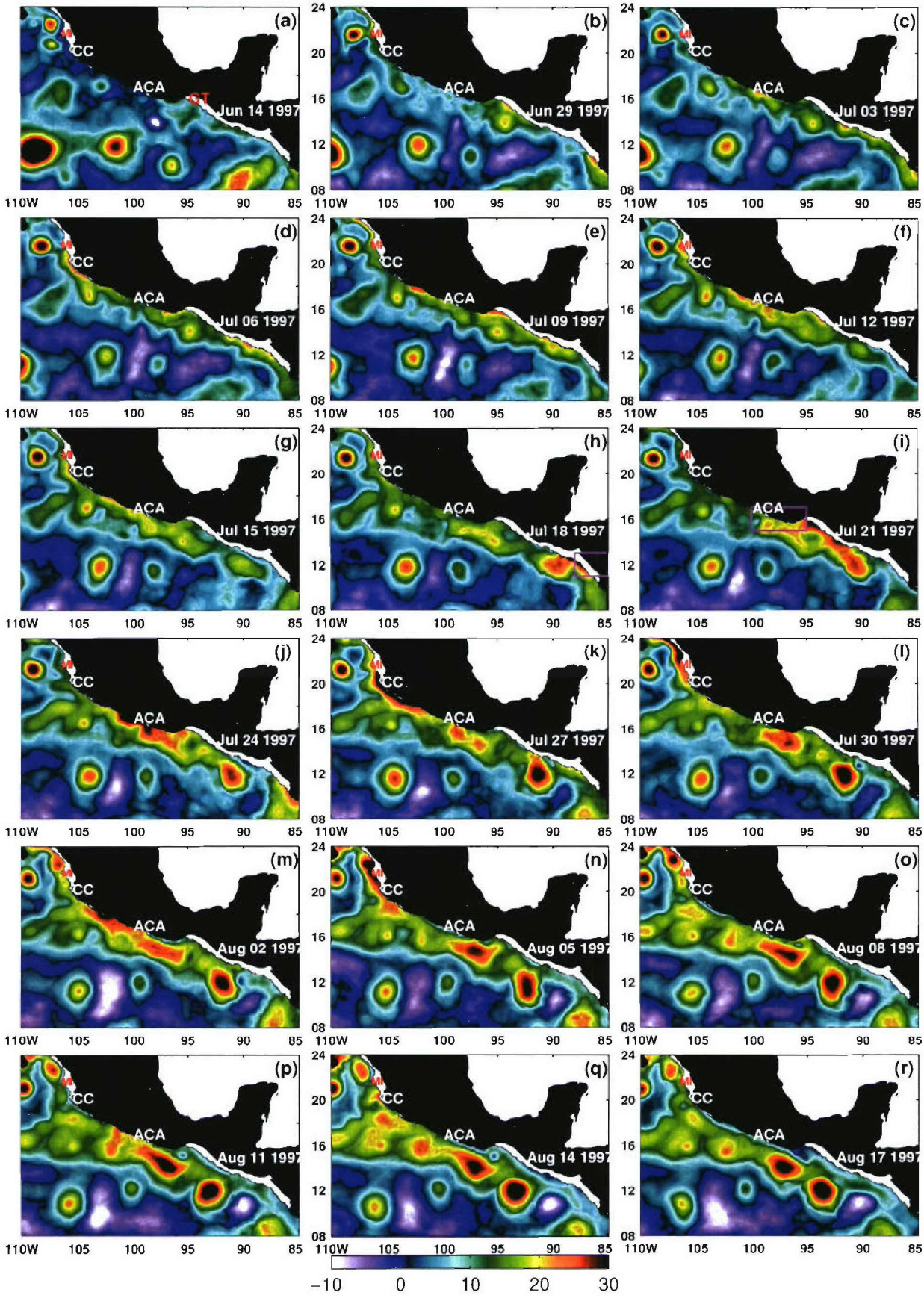
(a)
CC
ACA
GT
Jun 14 1997
(b)
Jun 29 1997
(c)
Jul 03 1997
(d)
Jul 06 1997
(e)
Jul 09 1997
(f)
Jul 12 1997
(g)
Jul 15 1997
(h)
Jul 18 1997
(i)
Jul 21 1997
(j)
Jul 24 1997
(k)
Jul 27 1997
(l)
Jul 30 1997
(m)
Aug 02 1997
(n)
Aug 05 1997
(o)
Aug 08 1997
(p)
Aug 11 1997
(q)
Aug 14 1997
(r)
Aug 17 1997
110W 105 100 95 90 85
24 20 16 12 08
−10 0 10 20 30

Figure 13

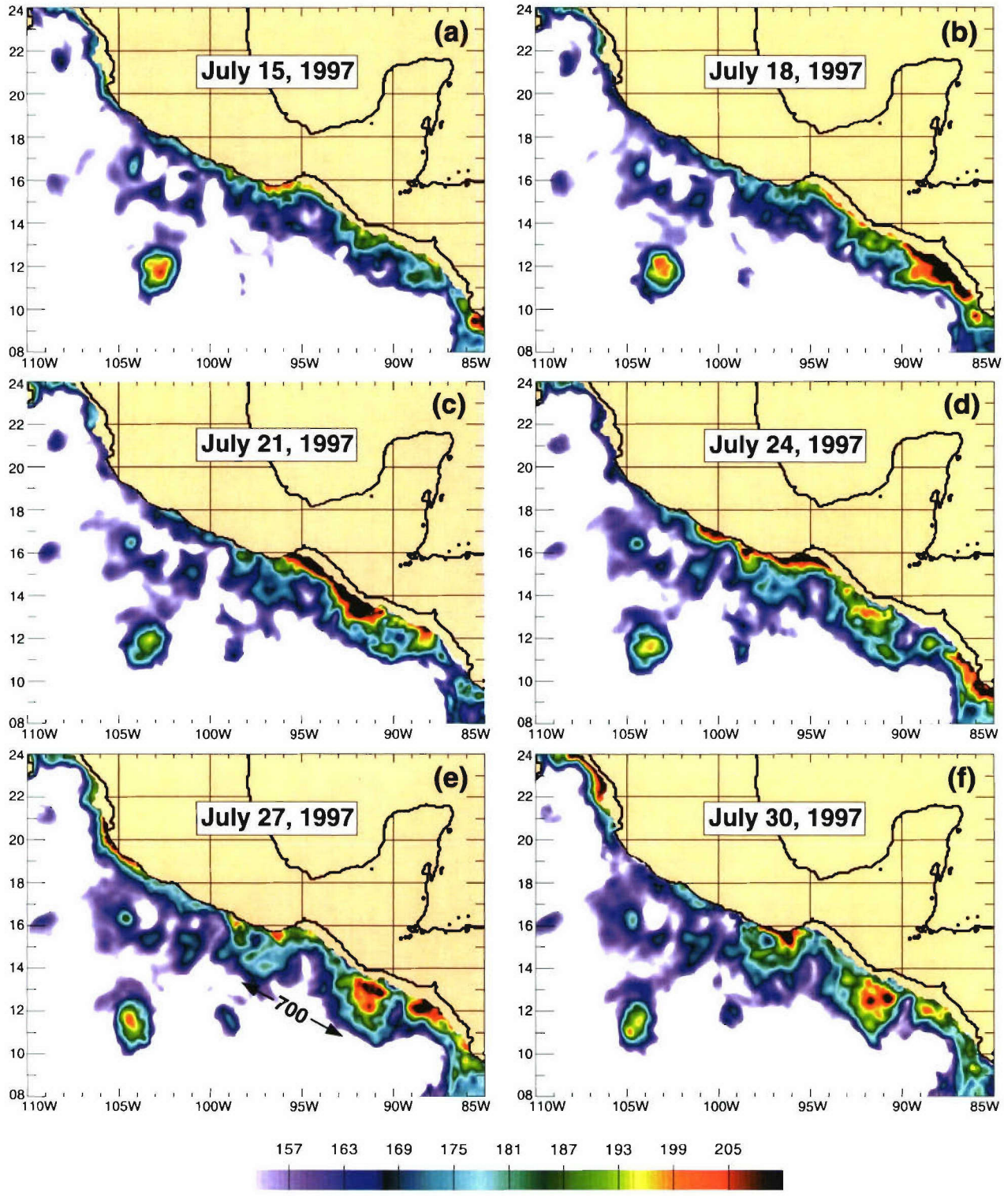

Figure 14. Layer 1 plus layer 2 thickness (color contours in m) for six different dates in July 1997 as simulated by 1/16° Pacific NLOM.

Figure 13. SSH anomaly (color contours in cm) for 18 different dates in June–August 1997 as simulated by 1/16° Pacific NLOM. The positions of the Gulf of Tehuantepec (GT), Acapulco (ACA), Cabo Corrientes (CC), and María Islands (MI) are indicated. The magenta box in Figure 13h indicates the area where the kinetic energy time series of Figure 15 were calculated.

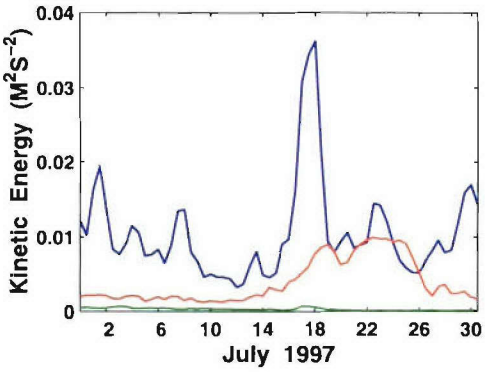

Figure 15. Time series of kinetic energy averaged over the magenta box shown in Figure 13h. The blue, red, and green time series correspond to the second layer (K_2) and the two lowest layers (K_5, and K_6), respectively.

clearly depicted in Figures 14a–14f. On 15 July 1997 the top two layer thickness includes a narrow and elongated feature (which is associated with the long-wavelength CTW) that is maximum along the coast, decays offshore, and is characterized by cross-shore and alongshore extensions of ~80 and ~3000 km for the positive anomaly, respectively (Figure 14a). Also, there is an anticyclonic eddy offshore centered near 103°W, 12°N. However, there is no anticyclonic eddy activity in the coastal areas northwest and southeast of the GT. Next, the short-wavelength CTW propagates through the GT region (Figures 14b–14e). Coincident with the passage of a short-wavelength CTW through the GT region, the long-wavelength CTW starts to meander (Figure 14c). It continues in an amplifying meander state (Figures 14c–14f) until anticyclonic eddies are generated northwest and southeast of the GT (Figure 14f). The alongshore wavelength of the meander is ~700 km (Figure 14e). That wavelength could be indicative of baroclinic instability. *Kundu* [1990] shows that in a 2-layer system, the wavelength with the fastest growth rate is $\sim 3.9 \cdot \pi \cdot R_1$ (where R_1 is the first baroclinic radius of deformation), which is ~735 km in our area of study, similar to the ~700 km wavelength simulated by NLOM (Figure 14e).

[24] As it propagates away from the coast, the long-wavelength CTW develops meanders at a wavelength consistent with baroclinic instability involving the barotropic mode. However, the evidence points toward internal mode baroclinic instability for the actual growth of the eddies, occurring when the short CTW passes through the area. This evidence is provided by kinetic energy and pressure fields. Figure 15 shows time series of kinetic energy in the second layer (K_2) and the lowest two layers (K_5, and K_6) during July 1997 for a region in the vicinity of the eddy southeast of the GT as outlined in Figure 13h. The large K_2 peak on 18 July is associated with the passage of the short-wavelength CTW through the region. It is noteworthy that of all the peaks in K_2, only the peak on 18 July has a corresponding increase in K_5, which is not reflected in K_6 (Figure 15). The decreasing K_2 accompanied by increasing K_5 and a basically invariant K_6 indicates a rapid transfer of energy from the upper to the lower baroclinic layers, a signature typical of internal mode baroclinic instability as clearly demonstrated, for example, by *Holland and Lin*

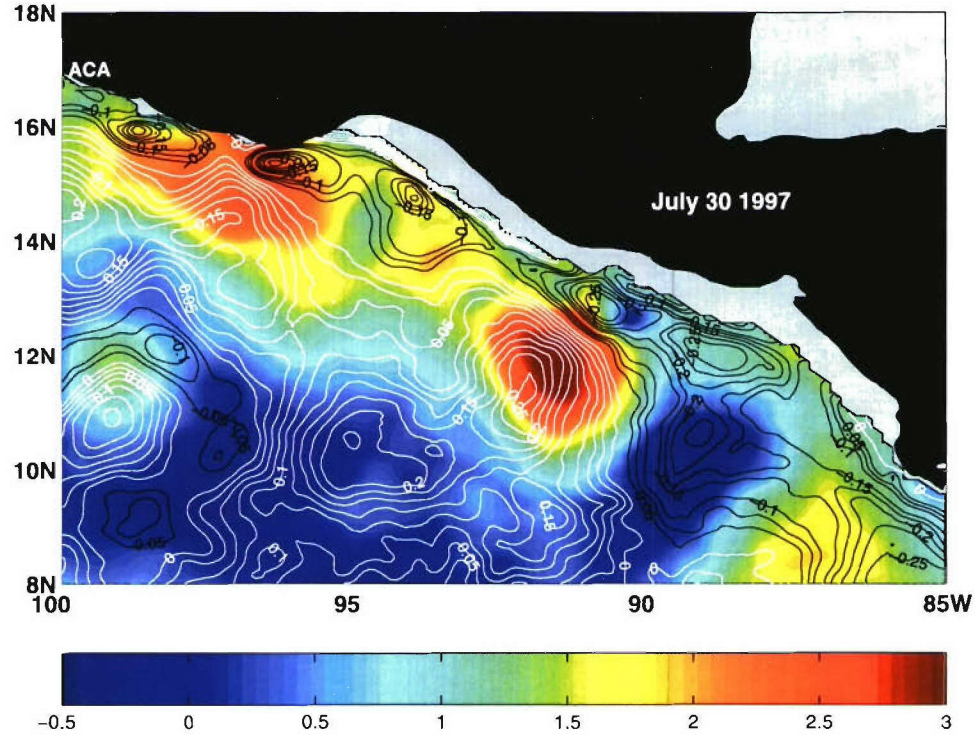

Figure 16. Surface layer pressure anomaly (color contours in m^2/s^2) overlain on layer 5 pressure (black (negative) and white (positive) contours in m^2/s^2) for 30 July 1997 as simulated by 1/16° Pacific NLOM. Note the phase lag in the vicinity of the eddies centered near 97°W, 14.8°N and 91.8°W, 12.0°N.

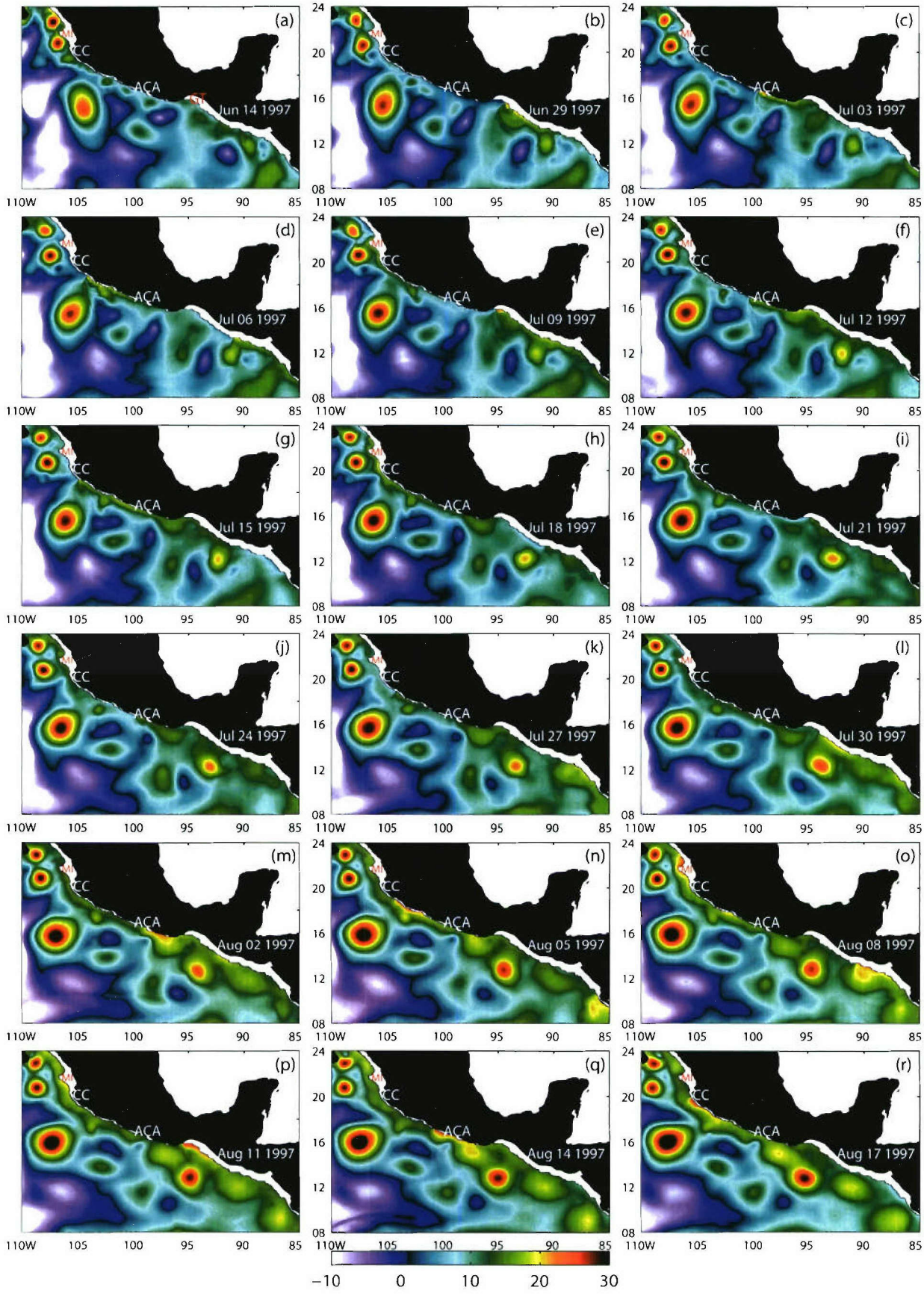
(a)
Jun 14 1997
(b)
Jun 29 1997
(c)
Jul 03 1997
(d)
Jul 06 1997
(e)
Jul 09 1997
(f)
Jul 12 1997
(g)
Jul 15 1997
(h)
Jul 18 1997
(i)
Jul 21 1997
(j)
Jul 24 1997
(k)
Jul 27 1997
(l)
Jul 30 1997
(m)
Aug 02 1997
(n)
Aug 05 1997
(o)
Aug 08 1997
(p)
Aug 11 1997
(q)
Aug 14 1997
(r)
Aug 17 1997
CC
ACA
110W 105 100 95 90 85
24 20 16 12 08
−10 0 10 20 30

Figure 17

[1975] and *Hurlburt et al.* [1990] for baroclinic instability involving the barotropic mode. The increase in K_5 on 18 July is a not a result of energy entering the subdomain through the boundaries. Furthermore, the surface layer pressure overlain on the fifth layer pressure (Figure 16) shows a significant phase difference between the two layers in the vicinity of the eddies centered near 97°W, 14.8°N, and 91.8°W, 12.5°N, again a characteristic of baroclinic instability. However, because of the pattern of vortex stretching and compression, propagating baroclinic eddies in general show a phase shift with depth. Thus we also investigate whether barotropic instability could be active in the formation of these eddies.

[25] The Beta Rossby numbers of the eddies centered near 91.8°W, 12.5°N (υ = 100 cm/s and $r \approx$ 146 km), and 97°W, 14.8°N (υ = 60 cm/s and $r \approx$ 160 km) are 2.0, and 1.2, respectively. Those numbers suggest a possible role for barotropic instabilities in the generation of these two eddies [*Hurlburt and Thompson*, 1982], but *Hurlburt et al.* [1996] found similar values in an eddy-resolving 5.5-layer reduced gravity model which allows internal mode baroclinic instability but excludes the barotropic mode. Then, to investigate further the possibility of barotropic instability, we performed a simulation using a 1.5-layer reduced gravity configuration. One of the big advantages of this simulation is that it does not include baroclinic instabilities but includes barotropic instabilities, allowing us to isolate the effects of the barotropic instabilities in the Tehuantepec eddy generation and modulation. The results of the 1.5-layer reduced gravity simulation show the formation of the two anticyclonic Tehuantepec eddies during July 1997 (Figure 17). Those eddies are weaker than the corresponding eddies in the 7-layer simulation with the maximum swirl velocity reduced to about 1/2. The Beta Rossby numbers of the eddies centered near 93°W, 12°N (υ = 60 cm/s and $r \approx$ 150 km), and 97.5°W, 15°N (υ = 30 cm/s and $r \approx$ 125 km) in Figure 17 are 1.2, and 1.0, respectively. Why are the eddies weaker in the 1.5-layer reduced gravity simulation when the eddies cannot pump energy to any other vertical mode as in the 7-layer simulation, and when consequently one might expect the generation of stronger rather than weaker eddies in the 1.5-layer reduced gravity simulation? The eddies in the 1.5-layer reduced gravity simulation are weak because they were not amplified by baroclinic instabilities, like the ones which imprint their signature in the kinetic energy time series of Figure 15. However, because these eddies developed, barotropic instabilities may contribute to the development of the anticyclonic eddies centered near 91.8°W, 12.5°N and 97°W, 14.8°N on 30 July 1997 (Figure 13) as well as baroclinic instabilities. Therefore, in this new generation mechanism for Tehuantepec eddies, the model results show that CTWs can trigger the development of mixed barotropic–internal mode–baroclinic instabilities and the instabilities trigger the development and/or amplification of the eddies.

[26] The contributions of long-wavelength and short-wavelength CTWs to the formation of Tehuantepec eddies during the summer of 1997 are summarized as follows. First, the long-wavelength CTW sets up the background conditions by deepening the coastal thermocline (Figure 14) and inducing poleward coastal currents. Next, the short-wavelength CTW strengthens the coastal poleward currents, producing strong horizontal and vertical shear of the velocity and triggering barotropic and baroclinic instabilities (Figures 15 and 16). This causes the long-wavelength CTW meanders to break, generating the two eddies (Figures 13 and 14). Since the long-wavelength CTW radiates energy westward in the form of Rossby waves, it contributes to the rapid detachment of the eddies from the coast, aided by an upwelling CTW which arrives around 14 August (Figure 13). The model results on CTWs as generators of Tehuantepec eddies are corroborated by model-independent analyses of satellite altimeter SSH data. The SSH anomalies from the Modular Ocean Data Assimilation System [*Fox et al.*, 2002] clearly show the arrival of the interannual CTW and the generation of two eddies southeast of the GT during summer of 1997 (Figure 18), results similar to the SSH anomalies simulated by NLOM (Figure 13).

3.3.4. Interannual Variability of Tehuantepec Eddies

[27] The GT winds as the main generator of the Tehuantepec eddies is unquestionable. On the other hand, the Tehuantepec and Papagayo winds do not show significant interannual variability (Figure 3), while the observed and modeled Tehuantepec eddies (Figure 2 and Table 1) and the intraseasonal CTWs do [*Enfield*, 1987; *Kessler et al.*, 1995]. Downwelling CTWs contribute to the generation and/or amplification of eddies by creating a more favorable ambient environment (deeper thermocline and larger positive SSH anomalies) and by triggering baroclinic and/or barotropic instabilities (sections 3.3.2 and 3.3.3). Hence these new generation mechanisms for Tehuantepec eddies have an intrinsic interannual variability (Table 1), which has been measured indirectly by the T/P altimeter and directly simulated by NLOM (Figure 2).

[28] El Niño and La Niña events, documented in Figure 2, are two opposite examples that indicate the importance of CTWs as a modulator of Tehuantepec eddy development. While the number and intensity of anticyclonic Tehuantepec eddies and intraseasonal downwelling CTWs increases (decreases) during El Niño (La Niña) years [*Kessler et al.*, 1995] (Figure 2 and Table 1), the GT and Papagayo winds are not significantly different during those events (Figure 3). Also, the mesoscale features documented in Figures 5–18 are examples that illustrate the roles of CTWs in Tehuantepec eddy formation and/or amplification. However, these are not unusual examples. Several other modeled years include similar cases where downwelling CTWs trigger anticyclonic eddies east and southeast of the GT. These new forcing mechanisms and region of generation (southeast of the GT) do not contradict, but complement the well-

Figure 17. SSH anomaly (color contours in centimeters) for 18 different dates in June–August 1997 as simulated by 1/16° Pacific NLOM (1.5-layer reduced gravity configuration). The positions of the Gulf of Tehuantepec (GT), Acapulco (ACA), Cabo Corrientes (CC), and María Islands (MI) are indicated.

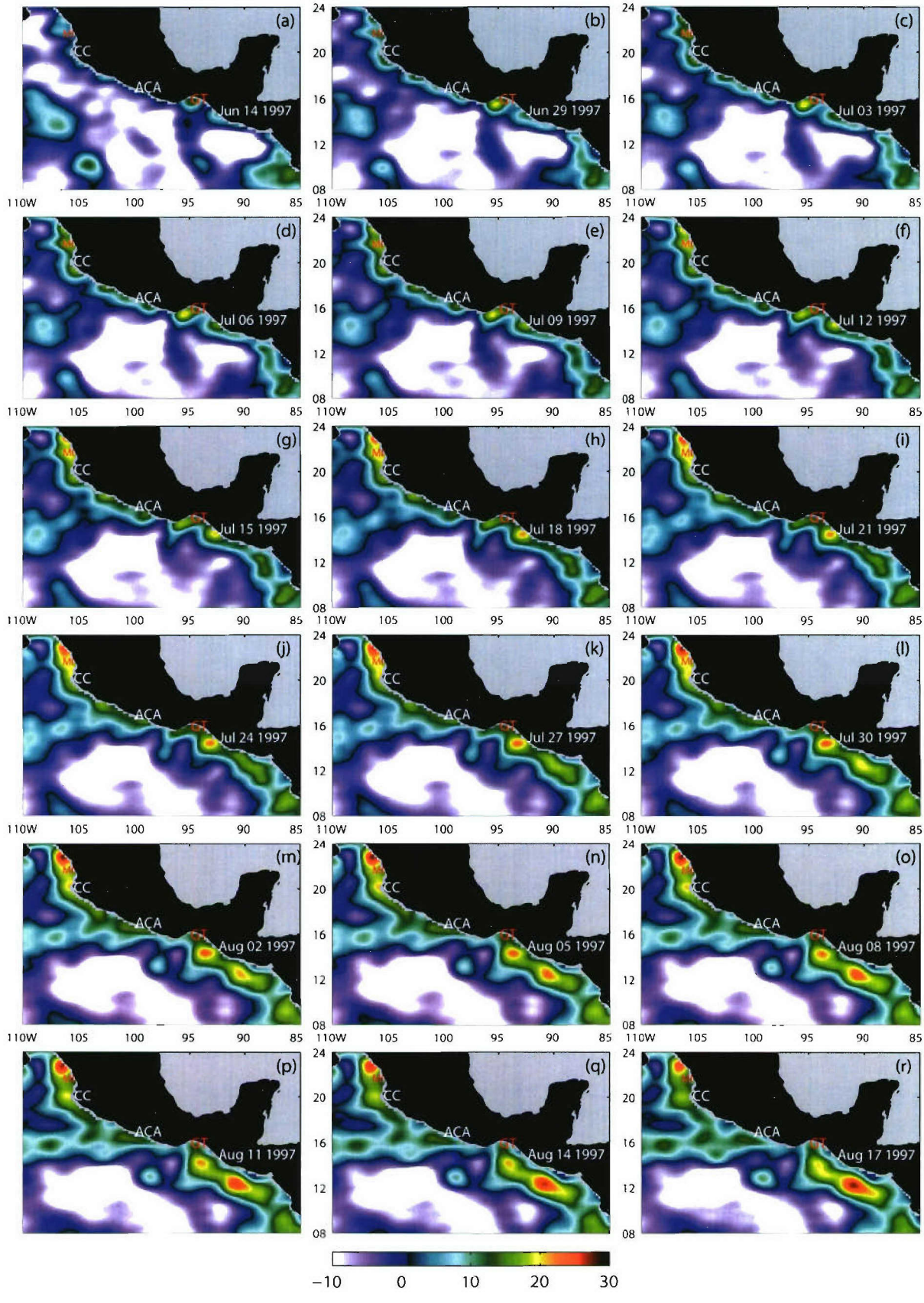

Figure 18. SSH anomaly (color contours in centimeters) for 18 different dates in June–August 1997 as produced by the Modular Ocean Data Assimilation System [*Fox et al.*, 2002]. The positions of the Gulf of Tehuantepec (GT), Acapulco (ACA), Cabo Corrientes (CC), and María Islands (MI) are indicated.

accepted theory of anticyclonic Tehuantepec eddies generated by strong wind events in the western GT.

4. Summary and Concluding Remarks

[29] For the first time Tehuantepec eddies have been studied using a high-resolution numerical ocean model forced with realistic interannual high-frequency winds. Results from the model and an almost 8-year time series, October 1992 to March 2000, of sea surface height measured by the TOPEX/Poseidon satellite altimeter show interannual variability in the number and strength of the Tehuantepec eddies (Figure 2 and Table 1). Demonstration of the Tehuantepec eddy interannual variability was made possible by the ability of the satellite altimeter to measure sea surface height during all weather, all seasons, and all oceanic conditions. A surprising and notable finding is that the altimeter measurements and the model results include anticyclonic Tehuantepec eddy formation during a 5-month period of weak Gulf of Tehuantepec winds throughout summer of 1997 (Figures 2, 3, 13, 14, 17, and 18), and anticyclonic eddy generation east and southeast of the Gulf of Tehuantepec (Figures 5, 8, 13, 14, 17, and 18). Additional examples of eddy generation in the area with strong Gulf of Tehuantepec winds are found in other years and other seasons of the same year. These new facts complement, but do not invalidate, the well-accepted theory of anticyclonic Tehuantepec eddy formation during fall/winter on the western side of the Gulf of Tehuantepec driven by strong Gulf of Tehuantepec wind events (Figures 5 and 6). Equally remarkable is that the model, which does not assimilate any oceanic data, reproduces qualitatively (Figure 2), and quantitatively (correlation coefficient of 0.72) the altimeter sea surface height observations.

[30] Opposite to our initial hypothesis, Tehuantepec eddy formation and Tehuantepec eddy interannual variability cannot be explained solely in terms of strong and intermittent Tehuantepec wind events (Figure 3). In fact, two different anticyclonic Tehuantepec eddy generation mechanisms are identified: first, the generation and modulation of the Tehuantepec eddies solely due to the Tehuantepec winds and, second, the anticyclonic Tehuantepec eddies generated by free propagating baroclinic intraseasonal and interannual downwelling coastally trapped waves. During their northward propagation and while propagating along the nonmeridional coasts of Central America and Mexico, these waves produce a strong horizontal and vertical shear of the horizontal velocity (Figure 11), and trigger barotropic and baroclinic instabilities in the flow (Figures 12 and 15–16) generating anticyclonic Tehuantepec eddies (Figures 5, 13, 14, 17, and 18). These equatorially generated waves have significant interannual variability increasing (decreasing) during El Niño (La Niña) years (Figures 7). In contrast, the Tehuantepec and Papagayo winds do not show a significant interannual variability (Figure 3). That suggests a dominant role for baroclinic downwelling coastally trapped waves in the modulation of the altimeter measured and model simulated Tehuantepec eddy interannual variability (Figure 2).

[31] **Acknowledgments.** This is a contribution to the 6.1 project Dynamics of Low Latitude Western Boundary Currents funded by the Office of Naval Research (ONR) under program element 601153N. L. Z. was funded by the 6.2 project Coastal Ocean Nesting Studies during the last part of this research. The numerical simulations were performed under the Department of Defense High Performance Computing Modernization Program on Cray T3E computers at the Naval Oceanographic Office, Stennis Space Center, Mississippi, and the Engineering Research and Development Center, Vicksburg, Mississippi. COAPS at the Florida State University receives its base support from an ONR Secretary of the Navy award to James J. O'Brien. In addition, we appreciate the helpful comments and suggestions of William Kessler, which led to improvements in the paper. This paper is NRL contribution number NRL/JA/7304-03-52.

References

Barton, E. D., M. L. Argote, J. Brown, P. M. Kosro, M. Lavín, J. M. Robles, R. L. Smith, A. Trasviña, and H. S. Velez (1993), Supersquirt: Dynamics of the Gulf of Tehuantepec, Mexico, *Oceanography*, *6*, 23–30.

Bourassa, M. A., L. Zamudio, and J. J. O'Brien (1999), Noninertial flow in NSCAT observations of Tehuantepec winds, *J. Geophys. Res.*, *104*, 11,311–11,319.

Chelton, D. B., M. H. Freilich, and S. K. Esbensen (2000a), Satellite observations of the wind jets off the Pacific Coast of Central America. part I: Case studies and statistical characteristics, *Mon. Weather Rev.*, *128*, 1993–2018.

Chelton, D. B., M. H. Freilich, and S. K. Esbensen (2000b), Satellite observations of the wind jets off the Pacific with center close to 91°W, 13.3°N coast of Central America. part II: Regional relationships and dynamical considerations, *Mon. Weather Rev.*, *128*, 2019–2043.

Clarke, A. J. (1998), Inertial wind path and sea surface temperature patterns near the Gulf of Tehuantepec and Gulf of Papagayo, *J. Geophys. Res.*, *93*, 15,491–15,501

Clarke, A. J., and C. Shi (1991), Critical frequencies at ocean boundaries, *J. Geophys. Res.*, *96*, 10,731–10,738.

Enfield, D. B. (1987), The intraseasonal oscillation in eastern Pacific sea levels: How is it forced?, *J. Phys. Oceanogr.*, *17*, 1860–1876.

European Center for Medium-Range Weather Forecasts (ECMWF) (1994), The Description of the ECMWF/WCRP level III—A global atmospheric data archive, report, 72 pp., Reading, U.K.

Fox, D. N., W. J. Teague, and C. N. Barron (2002), The Modular Ocean Data Assimilation System (MODAS), *J. Atmos. Oceanic Technol.*, *19*, 240–252.

Giese, B. S., J. A. Carton, and L. J. Holl (1994), Sea level variability in the eastern tropical Pacific as observed by TOPEX and Tropical Ocean-Global Atmosphere Tropical Atmosphere-Ocean Experiment, *J. Geophys. Res.*, *99*, 24,739–24,748.

Hansen, D. V., and G. A. Maul (1991), Anticyclonic current rings in the eastern tropical Pacific Ocean, *J. Geophys. Res.*, *96*, 6965–6979.

Holland, W. R., and L. B. Lin (1975), On the generation of mesoscale eddies and their contribution to the oceanic general circulation. I. A preliminary numerical experiment, *J. Phys. Oceanogr.*, *5*, 642–657.

Hurlburt, H. E., and J. D. Thompson (1980), A numerical study of Loop Current intrusions and eddy-shedding, *J. Phys. Oceanogr.*, *10*, 1611–1651

Hurlburt, H. E., and J. D. Thompson (1982), The dynamics of the Loop Current and shed eddies in a numerical model of the Gulf of Mexico, in *Hydrodynamics of Semi-Enclosed Seas*, edited by J. C. J. Nihoul, pp. 243–297, Elsevier Sci., New York.

Hurlburt, H. E., and J. D. Thompson (1984), Preliminary results from a numerical study of the New England Seamount Chain influence on the Gulf Stream, in *Predictability of Fluid Motions*, edited by G. Holloway, and B. J. West, pp. 489–504, Am. Inst. of Phys., College Park, Md.

Hurlburt, H. E., D. N. Fox, and E. J. Metzger (1990), Statistical inference of weakly correlated subthermocline fields from satellite altimeter data, *J. Geophys. Res.*, *95*, 11,375–11,409.

Hurlburt, H. E., P. J. Hogan, E. J. Metzger, W. J. Schmitz Jr., and A. J. Wallcraft (1996), Dynamics of the Kuroshio/Oyashio current system using eddy-resolving models of the North Pacific Ocean, *J. Geophys. Res.*, *101*, 941–976.

Japanese Meteorological Agency (JMA) (1991), Climate charts of sea surface temperatures of the western North Pacific and the global ocean, 51 pp., Mar. Div., Tokyo.

Kara, A. B., P. A. Rochford, and H. E. Hurlburt (2002), Air-sea flux estimates and the 1997–1998 ENSO event, *Boundary Layer Meteorol.*, *103*, 439–458.

Kelly, K. A., S. Dickinson, and Z. Yu (1999), NSCAT tropical wind stress maps: Implications for improving ocean modeling, *J. Geophys. Res.*, *104*, 11,291–11,310.

Kessler, W. S., M. J. McPhaden, and K. M. Weickmann (1995), Forcing of intraseasonal Kelvin waves in the equatorial Pacific, *J. Geophys. Res.*, *100*, 10,613–10,631

Kundu, P. K. (1990), *Fluid Mechanics*, 638 pp., Elsevier, New York.

Lavín, M. F., J. M. Robles, M. L. Argote, E. D. Barton, R. Smith, J. Brown, M. Kosro, A. Trasviña, H. S. Vélez Muñoz, and J. García (1992), Física del Golfo de Tehuantepec, *Rev. Cienc. Desarrollo, XVIII*, 97–108.

McCreary, J. P., Jr., H. S. Lee, and D. B. Enfield (1989), The response of the coastal ocean to strong offshore winds: With application to the Gulfs of Tehuantepec and Papagayo, *J. Mar. Res.*, *47*, 81–109.

McWilliams, J. C., and G. R. Flierl (1979), On the evolution of isolated nonlinear vortices, *J. Phys. Oceanogr.*, *9*, 1155–1182.

Melsom, A., S. D. Meyers, H. E. Hurlburt, E. J. Metzger, and J. J. O'Brien (1999), ENSO effects on Gulf of Alaska eddies, *Earth Interact.*, *3*, pap. 1. (Available at http://EarthInteractions.org.)

Melsom, A., E. J. Metzger, and H. E. Hurlburt (2003), Impact of remote oceanic forcing on Gulf of Alaska sea levels and mesoscale circulation, *J. Geophys. Res.*, *108*(C11), 3346, doi:10.1029/2002JC001742.

Metzger, E. J., and H. E. Hurlburt (2001), The nondeterministic nature of Kuroshio penetration and eddy shedding in the South China Sea, *J. Phys. Oceanogr.*, *31*, 1712–1732.

Müller-Karger, F. E., and C. Fuentes-Yaco (2000), Characteristics of wind-generated rings in the eastern tropical Pacific Ocean, *J. Geophys. Res.*, *105*, 1271–1284.

Murphy, S. J., H. E. Hurlburt, and J. J. O'Brien (1999), The connectivity of eddy variability in the Caribbean Sea, the Gulf of Mexico, and the Atlantic Ocean, *J. Geophys. Res.*, *104*, 1431–1453.

Murray, C. P., S. L. Morey, and J. J. O'Brien (2001), Interannual variability of upper ocean vorticity balances in the Gulf of Alaska, *J. Geophys. Res.*, *106*, 4479–4491.

Quadrelli, R., and J. M. Wallace (2002), Dependence of the structure of the Northern Hemisphere annular mode on the polarity of ENSO, *Geophys. Res. Lett.*, *29*(23), 2132, doi:10.1029/2002GL015807.

Romero-Centeno, R., J. Zavala-Hidalgo, A. Gallegos, and J. J. O'Brien (2003), Tehuantepec isthmus wind climatology and ENSO signal, *J. Clim.*, *16*, 2628–2639.

Rosmond, T. E., J. Teixeira, M. Peng, T. F. Hogan, and R. Pauley (2002), Navy Operational Global Atmospheric Predictions System (NOGAPS): Forcing for ocean models, *Oceanography*, *15*, 99–108.

Schultz, D. M., W. E. Bracken, L. F. Bosart, G. J. Hakim, M. A. Bedrick, M. J. Dickinson, and K. R. Tyle (1997), The 1993 superstorm cold surge: Frontal structure, gap flow, and tropical impact, *Mon. Weather Rev.*, *125*, 5–39.

Spall, M. A. (1992), Rossby wave radiation in the Cape Verde Frontal Zone, *J. Phys. Oceanogr.*, *22*, 796–807.

Spillane, M. C., D. B. Enfield, and J. S. Allen (1987), Intraseasonal oscillations in sea level along the west coast of the Americas, *J. Phys. Oceanogr.*, *17*, 313–325.

Trasviña, A., E. D. Barton, J. Brown, H. S. Velez, P. M. Kosro, and R. L. Smith (1995), Offshore wind forcing in the Gulf of Tehuantepec, Mexico: The asymmetric circulation, *J. Geophys. Res.*, *100*, 20,649–20,663.

Wallcraft, A. J. (1991), The Navy Layered Ocean Model users guide, *NOARL Rep.35*, 21 pp., Nav. Res. Lab., Stennis Space Cent., Miss.

Wallcraft, A. J., A. B. Kara, H. E. Hurlburt, and P. A. Rochford (2003), The NRL Layered Ocean Model (NLOM) with an embedded mixed layer submodel: Formulation and tuning, *J. Atmos. Oceanic Technol.*, *20*, 1601–1615.

Zamudio, L., A. P. Leonardi, S. D. Meyers, and J. J. O'Brien (2001), ENSO and eddies on the southwest coast of Mexico, *Geophys. Res. Lett.*, *28*, 13–16.

Zamudio, L., H. E. Hurlburt, E. J. Metzger, and O. M. Smedstad (2002), On the evolution of coastally trapped waves generated by Hurricane Juliette along the Mexican west coast, *Geophys. Res. Lett.*, *29*(23), 2141, doi:10.1029/2002GL014769.

H. E. Hurlburt and E. J. Metzger, Naval Research Laboratory, Code 7323, Stennis Space Center, MS 39529–5004, USA.

S. L. Morey, J. J. O'Brien, and L. Zamudio, Center for Ocean-Atmospheric Prediction Studies, Florida State University, Tallahassee, FL 32306–2840, USA. (luis.zamudio@nrlssc.navy.mil)

C. Tilburg, Department of Marine Sciences, University of Georgia, Athens, GA 30602, USA.

J. Zavala-Hidalgo, Centro de Ciencias de la Atmósfera, Universidad Nacional Autónoma de México, México, D. F.